9-23-2020

Functional, proteomic and bioinformatic analyses of Nrf2- and Keap1- null skeletal muscle

Lie Gao
University of Nebraska Medical Center

Vikas Kumar
University of Nebraska Medical Center

Neetha Nanoth Vellichirammal
University of Nebraska Medical Center

Song-young Park
University of Nebraska at Omaha, song-youngpark@unomaha.edu

Tara L. Rudebush
University of Nebraska Medical Center

Follow this and additional works at: https://digitalcommons.unomaha.edu/hperfacpub

Part of the Health and Physical Education Commons, and the Kinesiology Commons
Please take our feedback survey at: https://unomaha.az1.qualtrics.com/jfe/form/
SV_8cchtFmpDyGfBLE

Recommended Citation

Gao, L., Kumar, V., Vellichirammal, N.N., Park, S.-Y., Rudebush, T.L., Yu, L., Son, W.-M., Pekas, E.J., Wafi, A.M., Hong, J., Xiao, P., Guda, C., Wang, H.-J., Schultz, H.D. and Zucker, I.H. (2020), Functional, proteomic and bioinformatic analyses of Nrf2- and Keap1- null skeletal muscle. J Physiol, 598: 5427-5451. https://doi.org/10.1113/JP280176

Authors

Lie Gao, Vikas Kumar, Neetha Nanoth Vellichirammal, Song-young Park, Tara L. Rudebush, Li Yu, Won-Mok Son, Elizabeth J. Pekas, Ahmed M. Wafi, Juan Hong, Peng Xiao, Chittibabu Guda, Han-Jun Wang, Harold D. Scultz, and Irving H. Zucker

Functional, proteomic and bioinformatic analyses of Nrf2- and Keap1- null skeletal muscle

Lie Gao[1], Vikas Kumar[2], Neetha Nanoth Vellichirammal[3], Song-Young Park[4], Tara L. Rudebush[1], Li Yu[1], Won-Mok Son[4], Elizabeth J. Pekas[4], Ahmed M. Wafi[1], Juan Hong[6], Peng Xiao[3,5], Chittibabu Guda[3,5], Han-Jun Wang[6], Harold D. Schultz[1], and Irving H. Zucker[1]

[1]Department of Cellular & Integrative Physiology, University of Nebraska Medical Center, Omaha, NE, USA

[2]Mass Spectrometry & Proteomics Core, University of Nebraska Medical Center, Omaha, NE, USA

[3]Department of Genetics, Cell Biology and Anatomy, University of Nebraska Medical Center, Omaha, NE, USA

[4]School of Health and Kinesiology, University of Nebraska Omaha, Omaha, NE, USA

[5]Bioinformatics and Systems Biology Core, University of Nebraska Medical Center, Omaha, NE, USA

[6]Department of Anesthesiology, University of Nebraska Medical Center, Omaha, NE, USA

Lie Gao and Vikas Kumar contributed equally to this work.

Edited by: Kim Barrett & Russell Hepple

Abstract

Although Nrf2 has been recognized as a master regulator of cytoprotection, its functional significance remains to be completely defined. We hypothesized that proteomic/bioinformatic analyses from Nrf2-deficient or overexpressed skeletal muscle tissues will provide a broader spectrum of Nrf2 targets and downstream pathways than are currently known. To this end, we created two transgenic mouse models; the iMS-$Nrf2^{flox/flox}$ and iMS-$Keap1^{flox/flox}$, employing which we demonstrated that selective deletion of skeletal muscle Nrf2 or Keap1 separately impaired or improved skeletal muscle function. Mass spectrometry revealed that Nrf2-KO changed expression of 114 proteins while Keap1-KO changed expression of 117 proteins with 10 proteins in common between the groups. Gene ontology analysis suggested that Nrf2 KO-changed proteins are involved in metabolism of oxidoreduction coenzymes, purine ribonucleoside triphosphate, ATP and propanoate, which are considered as the basal function of Nrf2, while Keap1 KO-changed proteins are involved in cellular detoxification, NADP metabolism, glutathione metabolism and the electron transport chain, which belong to the induced effect of Nrf2. Canonical pathway analysis suggested that Keap1-KO activated four pathways, whereas Nrf2-KO did not. Ingenuity pathway analysis further

revealed that Nrf2-KO and Keap1-KO impacted different signal proteins and functions. Finally, we validated the proteomic and bioinformatics data by analysing glutathione metabolism and mitochondrial function. In conclusion, we found that Nrf2-targeted proteins are assigned to two groups: one mediates the tonic effects evoked by a low level of Nrf2 at basal condition; the other is responsible for the inducible effects evoked by a surge of Nrf2 that is dependent on a Keap1 mechanism.

Key points

- Nrf2 is a master regulator of endogenous cellular defences, governing the expression of more than 200 cytoprotective proteins, including a panel of antioxidant enzymes.

- Nrf2 plays an important role in redox haemostasis of skeletal muscle in response to the increased generation of reactive oxygen species during contraction.

- Employing skeletal muscle-specific transgenic mouse models with unbiased-omic approaches, we uncovered new target proteins, downstream pathways and molecular networks of Nrf2 in skeletal muscle following Nrf2 or Keap1 deletion.

- Based on the findings, we proposed a two-way model to understand Nrf2 function: a tonic effect through a Keap1-independent mechanism under basal conditions and an induced effect through a Keap1-dependent mechanism in response to oxidative and other stresses.

Lie Gao studied clinical medicine at the West China Medical Centre of Sichuan University and then physiology at Peking Union Medical College where he received a PhD degree. He is an Assistant Professor in the Department of Cellular and Integrative Physiology at the University of Nebraska Medical Centre. His research has been involved in neural control of sympathetic activity in hypertension and chronic heart failure, with a focus on oxidative stress and Angiotensin II. He is also interested in the redox biology of skeletal muscle under the governance of the Nrf2/Keap1 system. He has authored over 60 peer-reviewed publications in

peer-reviewed journals. **Vikas Kumar** received his PhD from the University of Otago, New Zealand (2011), studying cardiac redox proteomics changes. He then did his post-doctoral training through the Cardiovascular Proteomics Centre at the Boston University School of Medicine. He has over 10 years of experience in the field of mass spectrometry-based proteomics. He has designed and executed experiments for global proteomics profiling, quantitative proteomics and PTMs (phosphorylation, oxidative post-translational modifications, HNE, acetylation) analysis. Furthermore, he is well versed in many of the available data analysis and pathway analysis software packages. Vikas has developed a novel method for estimating reversible thiol oxidation and its site occupancy using iodo-Tandem Mass Tags strategy. Vikas is using a proteomics approach to understand how oxidative changes regulate physiology and pathophysiology.

Introduction

        The nuclear factor erythroid-derived 2 (Nrf2)/Kelch ECH-associating protein 1 (Keap1) complex is a redox-sensitive transcriptional regulatory system where Keap1 functions as a sensor of reactive oxygen species (ROS) and electrophiles, while Nrf2 serves as an effector for the coordinated activation of a battery of cytoprotective genes that encode proteins involved in anti-oxidation, anti-inflammation, detoxification and metabolism (Yamamoto *et al*. 2018). Under basal conditions, Nrf2 is sequestered in the cytoplasm by Keap1 to be rapidly degraded via the ubiquitin-proteasomal system, thereby keeping antioxidant enzymes at a relatively low level. When intracellular ROS rises, several Cys residues of the Keap1 molecule are oxidized, leading to Nrf2 liberation from association with Keap1 and trans- location to the nucleus where Nrf2 binds to antioxidant response elements (AREs) and stimulates antioxidant enzyme gene expression (Bruns *et al*. 2015). Nrf2/Keap1 therefore plays a critical role in the maintenance of intra- cellular redox homeostasis (Lee *et al*. 2005; Osburn & Kensler, 2008; Hayes & Dinkova-Kostova, 2014).

        Skeletal muscle is a highly dynamic organ with a wide range of functions and metabolism. Skeletal myocyte oxygen consumption and ROS generation are low in the sedentary state but dramatically increased during strenuous aerobic exercise (Kanter, 1998; Powers & Hamilton, 1999; Urso & Clarkson, 2003). Muscle-derived ROS includes O_2^-, H_2O_2, ·OH and other highly reactive oxidants (McArdle *et al*. 2001; Pattwell *et al*. 2004; Jackson, 2008; Powers & Jackson, 2008; Jackson, 2011), which have high potential to damage cellular constituents by oxidizing proteins, nucleic acids and lipids (Davies *et al*. 1982; Duthie *et al*. 1990; Reid *et al*. 1992*a,b*). In order to overcome this challenge, skeletal myocytes have developed powerful endogenous antioxidant defences consisting of enzymatic and non-enzymatic antioxidants (Steinbacher & Eckl, 2015), most of which are governed by the Nrf2/Keap1 system. It has been demonstrated that electrical stimulation of C2C12 cells, a skeletal muscle cell line, activates Nrf2, leading to marked upregulation of NQO1, HO-1 and GCLm, that was abolished when *Nrf2* was deleted using siRNA (Horie *et al*. 2015). Acute treadmill exercise in mice evoked Nrf2 release from the Nrf2/Keap1 complex and translocation into the nucleus of skeletal myocytes, significantly upregulating SODs, Cat, HO-1, GCLc and GCLm gene expression (Li *et al*. 2015). On the other hand, Nrf2-deficient mice exhibit a significantly lower antioxidant enzyme abundance and higher ROS levels in skeletal muscle as compared with age-matched wild-type controls (Miller *et al*. 2012). Exercise performance and muscle contractility of Nrf2-deficient mice were also impaired (Crilly *et al*. 2016; Merry & Ristow, 2016). However, most investigations on *Nrf2* signaling were carried out by using

candidate gene/protein approaches, such as polymerase chain reaction and immunoblotting that restricts the exploration of unknown areas of this potent transcription factor, since specific targets have been pre-selected.

In the present study, we hypothesized that proteomic and bioinformatic analyses of skeletal muscle with Nrf2 deficiency or overexpression uncovers novel targets and will provide a broader understanding of Nrf2 downstream pathways. To this end, we created two skeletal muscle-specific transgenic mouse models, iMS-*Nrf2*^{flox/flox} and iMS-*Keap1*^{flox/flox}, by crossing mice expressing the human *α*-skeletal actin promoter-driven Cre-recombination with mice expressing floxed *Nrf2* or *Keap1* genes. Employing these two models, we determined the impact of *Nrf2* deletion or overexpression (i.e. *Keap1* knockout) on skeletal muscle function, proteomic profiles and molecular signalling networks to uncover novel target proteins and downstream signaling pathways of Nrf2 in skeletal muscle.

Materials and methods

Generation of inducible skeletal muscle-specific *Nrf2* and *Keap1* inactivation models: iMS-*Nrf2*^{flox/flox} and iMS-*Keap1*^{flox/flox} mice

All animal procedures were conducted in accordance with the guidelines of the National Institutes of Health *Guide for the Care and Use of Laboratory Animals* and conformed to *ARRIVE Guidelines* (https://www.nc3rs.org.uk/arrive-guidelines), as approved by the Animal Care and Use Committee of the University of Nebraska Medical Centre (UNMC-IACUC Protocol #18-174-02). The iMS-*Nrf2*^{flox/flox} and iMS-*Keap1*^{flox/fox} mice were produced by crossing the HSA-MCM line with Nrf2^{flox/flox} and Keap1^{flox/flox} lines. The HSA-MCM mouse, a skeletal muscle-specific Cre-recombinase mouse line, was purchased from the Jackson Laboratory ([STOCK Tg(ACTA1-cre/Esr1∗)2Kesr/J]; Stock No: 025750) that was originally created by McCarthy *et al*. at the University of Kentucky (McCarthy *et al*. 2012). This strain expresses MerCreMer double fusion protein (a mutated oestrogen receptor ligand-binding domain at both the N- and C-termini) under the control of the human skeletal muscle ACTA1 promoter. Cre-mediated recombination is restricted to skeletal muscles and induced exclusively by tamoxifen. Dr Shyam Biswal of the Johns Hopkins University provided the Nrf2^{flox/flox} and Keap1^{flox/flox} mice containing LoxP sites flanking exon 5 of the *Nrf2* gene or exons 2 and 3 of the *Keap1* gene and are indistinguishable from wild-type littermates (Kong *et al*. 2011). Breeding these HSA-MCM mice with the Nrf2^{flox/flox} and Keap1^{flox/flox} mice generated offspring in which selective deletion of the DNA-binding domain of *Nrf2* and intervening Kelch domains of

Keap1 in skeletal muscle could be induced upon tamoxifen administration. Inducible skeletal muscle-specific *Nrf2* and *Keap1* knockout mice were generated as previously described (Hodge *et al*. 2015) with the following modification: female Nrf2*flox/flox* and Keap1*flox/flox* mice were crossed with male HSA-MCM mice to yield an F1 generation of skeletal muscle-specific *Cre*^{+/−};*Nrf2*[+/flox] and *Cre*^{+/−};*Keap1*[+/flox] mice. Breeding the F1 generation males to the Nrf2*flox/flox* and Keap1*flox/flox* females resulted in the skeletal muscle-specific *Cre*^{+/−};*Nrf2*[flox/flox] and *Cre*^{+/−};*Keap1*[flox/flox] mice (referred to as iMS-*Nrf2*[flox/flox] and iMS-*Keap1*[flox/flox]) needed for this study.

Cre-loxP recombination induction of skeletal muscle-specific *Nrf2* or *Keap1* gene inactivation

Activation of Cre-recombination was carried out by intraperitoneal injections of tamoxifen (Tam, 2 mg/0.2 ml day^{-1}, Sigma-Aldrich, St. Louis, MO, USA; Cat. No. T5648) for five consecutive days when the mice reached 12 weeks of age. Controls were vehicle (Veh, 15% ethanol in sunflower seed oil, 0.2 ml day^{-1} for 5 days)-treated mice. To avoid potential activation of endogenous oestrogen on Cre-recombination, only male mice were used in these experiments. Twenty weeks post-injection, mice were assigned to two cohorts for functional evaluation and proteomic analyses.

Maximal exercise capacity

Exercise performance was evaluated as previously described from our laboratory (Wafi *et al*. 2018). Briefly, mice were exposed to a treadmill for 20 min, once a day, for 3 days prior to the first exercise evaluation. On the day of the test, mice were placed on the treadmill which was supplied with an electrical grid at the rear (stimulus: 5 Hz, 5 V). Exercise was initiated at a speed of 6 m min^{-1} for 6 min at an inclination of 15°, followed by an increase of 3 m min^{-1} every 3 min until exhaustion, as defined when mice remained on the electrical grid for 20 s without attempting to re-engage the treadmill.

In situ muscle contractility

This assessment was performed *in situ* on the soleus (Sol, oxidative muscle), extensor digitorum longus (EDL, glycolytic muscle) and gastrocnemius (Gas, mixed muscle) muscles, as described previously (Wafi *et al*. 2018). In brief, under 2% isoflurane anaesthesia, mice were placed on a heated surgical table in the prone position. A small incision in the skin above the calf was made and the Sol, EDL and Gas were identified. The proximal tendon of the Sol and the distal tendons of the EDL and Gas were isolated, cut and sutured with a #6 silk suture, by which the tendons were attached to a force transducer (MLT1030/A, ADInstruments, Inc., Colorado Springs, CO, USA) with muscles kept at their *in situ* length. Muscle

contraction was evoked by intermittent tetanic stimulation with trains of square wave pulses (2.5 V, 0.3 s at 50 Hz per 3 s for a total of 20 min) delivered by a pulse generator (A310 Accupulser, World Precision Instruments; Sarasota, FL, USA). The force of contraction was recorded by a Powerlab system and LabChart software. The data were saved in a PC using LabChart 7.0 software (ADInstruments, Colorado Springs, CO, USA). During the experiment, mice were kept warm by an isothermal pad and heat lamp while the muscles and tendons were moisturized by periodic administration of warm saline.

Animal killing and sample collection

After weighing for body mass, mice were anaesthetized with 2% isoflurane. Blood was collected by cardiac puncture into a 1.5 ml Eppendorf tube containing 2% EDTA. The anti-coagulated blood was centrifuged for 5 min at 15,000 g at 4˚C to harvest plasma, which was stored at −80°C. Mice were then killed by administration of 5% isoflurane until 1 min after breathing stopped. The mice were decapitated and the whole brain was harvested. After removing the cerebellum and cerebrum, the brain- stem was stored at −80°C. Bilateral Sol, EDL and Gas were removed from the hindlimb, weighed and stored at−80°C.

Western blot analyses

Skeletal muscle tissues were homogenized in Radio- immunoprecipitation assay (RIPA) buffer (50 mM TrisHCl pH7.4, 150 mM NaCl, 2 mM EDTA, 1% NP-40, 0.1% SDS) with 1% protease inhibitor cocktail (Abcam, ab65621, Cambridge, UK), from which total protein was extracted by centrifuging at 20,000 g. The protein concentration of extract was measured using a protein assay kit (Pierce; Rockford, IL, USA) and then adjusted to equal volume in all samples with 2 × 4% SDS sample buffer. The samples were boiled for 5 min and then loaded on a 7.5% SDS-PAGE gel (30 μg protein/10 μl per well) followed by electrophoresis using a Bio-Rad mini gel apparatus at 40 mA/gel for 45 min. The fractionated protein on the gel was electrically transferred onto a polyvinyl difluoride membrane (Millipore). The membrane was first probed with the primary anti- bodies (Nrf2 ab137550, Keap1 sc-33569, HO-1 ab68477, NQO1 ab80588, SOD2 sc-30080, SOD1 sc-8637, Catalase sc-50508, GPX ab22604, GR ab124995, TrxR1 ab124954, GSTA2 ab232833, GSTA4 ab231601 and total OXPHOS ab110413; from Abcam 'ab' and Santa Cruz Biotechnology 'sc') and the secondary antibody (HRP goat anti-rabbit IgG antibody and HRP goat anti-mouse IgG, HRP, Thermo-Fisher Scientific, Waltham, MA, USA). After three washes with tris-buffered saline Tween (TBST), the membrane was treated with enhanced chemiluminescence substrate (Pierce; Rockford, IL, USA) for 5 min. The blots on the membrane were visualized and analysed using a UVP BioImaging System (EpiChemi II Darkroom). The

membranes were then treated with restore western blot stripping buffer (Thermo Scientific) to remove the blots, followed by probing with glyceraldehyde-3-phosphate dehydrogenase (GAPDH) primary antibodies (sc-32233) to obtain GAPDH blots as an internal control. The final reported data are the normalized target protein band densities divided by GAPDH. In the last five western blots, the target bands (GR, TrxR1, GSTA2, GSTA4 and mitochondrial OXPHOS) were normalized by Ponceau S staining. The western blot was completed by a technician blinded to the groups, following the established guidelines to validate the antibodies (Brooks & Lindsey, 2018).

Glutathione assays

Reduced (GSH) and oxidized (GSSG) glutathione from gastrocnemius and brainstem were assessed employing a glutathione fluorescent detection assay kit (BioVision, Milpitas, CA, USA). Following the manufacturer's instructions, 20 mg tissue was homogenized in 200 μl pre-cold glutathione assay buffer, from which 60 μl homogenate (or 60 μl plasma for blood glutathione assay) was taken to mix with 20 μl 6N perchloric acid. After being kept on ice for 5 min and centrifugation at 13,000 g for 2 min, 40 μl supernatant was mixed with 20 μl pre-cold 6N KOH. The sample was then kept on ice for 5 min and centrifuged again at 13,000 g for 2 min. Ten micro-litres of supernatant were used to detect GSH or GSSG by mixing with the fluorescent probe or the fluorescent probe plus quencher and reducing agent. Fluorescence was measured at Ex/Em = 340/420 nm using a Tecan Infinite 200 fluorescent microplate reader (Tecan Group Ltd., Switzerland).

Skeletal muscle mitochondrial respiratory functional assessment

Immediately upon excision the Sol and EDL were placed in ice-cold buffer A containing (in mM) 2.77 CaK2EGTA, 7.23 K2EGTA, 6.56 MgCl2, 0.5 dithiothreitol (DTT), 50 K-MES, 20 imidazole, 20 taurine, 5.77 Na2ATP and 15 phosphocreatine at pH 7.1 for 30 min. Next, being shaken mildly for 40 min in buffer A supplemented with 50 μg ml^{-1} saponin, the muscle was rinsed (2 × 10 min/rinse) in buffer B containing (in mM) 2.77 CaK2EGTA, 7.23 K2EGTA, 6.56 MgCl2, 0.5 DTT, 50 K-MES, 20 imidazole, 20 taurine, 5.77 ATP and 15 phosphocreatine at pH 7.0 (Park *et al*. 2014). Mitochondrial respiration was assessed by measuring the oxygen consumption rate in buffer B, while being continuously stirred, at 37°C using a high-resolution Oxygraph-2k (Oroboros, Austria, Innsbruck) as previously described (Park *et al*. 2014). Briefly, after the baseline respiration rate in the absence of substrate was recorded: 1) complex I state 2 respiration was assessed in the presence of glutamate + malate; 2) complex I state 3 respiration, the ADP-stimulated state of oxidative phosphorylation, was measured in the presence of glutamate + malate + ADP; and 3) complex

I + II state 3 respiration was evaluated in the presence of glutamate + malate + ADP + succinate (Park et al. 2016). In all experiments, the integrity of the outer mitochondrial membrane was confirmed by cytochrome c injection after the assessment of complex I and II state 3 respiration. None of the samples exhibited an increase in the rate of oxygen consumption following the addition of cytochrome c (data not shown). After respiratory measurements, muscle samples were snap-frozen and citrate synthase (CS) activity was determined (Park et al. 2016). It should be noted that state 2 respiration was determined in the presence of glutamate + malate (in the absence of the complex II substrate succinate, since complex II does not release protons to the intermembrane space). Importantly, no difference was observed for state 2 respiration when comparing glutamate + malate + succinate vs. glutamate + malate as substrates (data not shown). For measurement of state 3 respiration, ADP and succinate were supplemented in the respiration buffer to prevent depletion of metabolites from the mitochondrial matrix and to reconstitute the tricarboxylic acid cycle (Gnaiger, 2009; Park et al. 2014; Gifford et al. 2015). Concentrations of each reagent in the vessel chamber were glutamate (2 mM), malate (10 mM), ADP (5 mM), succinate (10 mM) and cytochrome c (10 μM) (Park et al. 2014). Carbonyl cyanide-4(trifluoromethoxy)phenylhydrazone (FCCP, 0.6–1 μM) and potassium cyanide (KCN, 10 mM) were used for complex IV respiration.

Mitochondria content marker (citrate synthase activity)

Measurement of CS activity: frozen muscle samples previously used for mitochondrial respiration measurements were homogenized (in mM: 250 sucrose, 40 KCl, 2 EGTA and 20 Tris·HCl, pH 7.4). The homogenates were then supplemented with 0.1% Triton X-100 and incubated on ice for 60 min followed by centrifugation for 8 min at 10,000 g and a 20× dilution (Park et al. 2014). Similarly, the muscle was homogenized followed by two freeze–thaw cycles to release the CS from the mitochondrial matrix, followed by centrifugation for 10 min and a 10× dilution (Park et al. 2014). CS activity was determined in a total reaction volume of 1 ml for muscle homogenates. The reaction was performed in reaction buffer containing (in mM) 220 sucrose, 40 KCl, 20 HEPES, 1 EGTA, 0.1 5,5'-dithio-bis-2-nitrobenzoic acid (DTNB) and 0.1 acetyl-CoA, pH 7.4 at 25°C and was started by the addition of 0.05 mM oxaloacetate. CS activity was monitored at 412 nm to detect the reaction of sulfhydryl groups of CoA with DTNB for a total duration of 3 min using an Ultrospec 3000 spectrophotometer (Amersham Pharmacia Biotech, Amersham, UK).

Mass spectrometry-based proteomics

Mice were killed by inhalation of CO_2. The Sol and EDL were collected and snap-frozen in liquid nitrogen. Samples were homogenized in RIPA buffer (50 mM TrisHCl, 195 mM NaCl, 2 mM

EDTA, 1% NP-40, 0.1% SDS) with 1% protease inhibitor cocktail (Abcam, ab65621), and the protein extracted by centrifuging at 20,000 g at 4°C for 20 min. Protein concentration was quantified by protein assay (Pierce; Rockford, IL, USA). Fifty micrograms of protein per sample from three biological replicates per group was reduced and alkylated with 10 mM DTT at 55°C and 50 mM iodoacetamide at room temperature, respectively. Detergent was removed by chloroform/methanol extraction, and the protein pellet was re-suspended in 50 mM ammonium bicarbonate and digested with MS-grade trypsin (Pierce) overnight at 37°C. Peptides cleaned with PepClean C18 spin columns (Thermo) were re-suspended in 2% acetonitrile (ACN) and 0.1% formic acid (FA) and 500 ng of each sample was loaded onto trap column Acclaim PepMap 100 75 μm × 2 cm C18 LC Columns (Thermo Scientific) at a flow rate of 4 μl min^{-1} then separated with a Thermo RSLC Ultimate 3000 (Thermo Scientific) on a Thermo Easy-Spray PepMap RSLC C18 75 μm × 50 cm C-18 2 μm column (Thermo Scientific) with a step gradient of 4–25% solvent B (0.1% FA in 80 % ACN) from 10–130 min and 25–45% solvent B for 130–145 min at 300 nl min^{-1} and 50°C with a 180 min total run time. Eluted peptides were analysed by a Thermo Orbitrap Fusion Lumos Tribrid (Thermo Scientific) mass spectrometer in a data-dependent acquisition mode. A survey full scan MS (from m/z 350–1800) was acquired in the Orbitrap with a resolution of 120,000. The automatic gain control (AGC) target for precursor ion scan (MS1) was set as 4 × 105 and ion filling time set at 100 ms. The most intense ions with charge state 2–6 were isolated in 3 s cycles and fragmented using higher energy collisional dissociation fragmentation with 35% normalized collision energy and detected at a mass resolution of 30,000 at 200 m/z. The AGC target for MS/MS was set at 5 × 10^4 and ion filling time set 60 ms dynamic exclusion was set for 30 s with a 10 ppm mass window. Protein identification was performed by searching MS/MS data against the Swiss-prot mus musculus protein database downloaded on 13 February 2019 using the in-house mascot 2.6.2 (Matrix Science, Boston, MA, USA) search engine. The search was set up for full tryptic peptides with a maximum of two missed cleavage sites. Acetylation of protein N-terminus and oxidized methionine were included as variable modifications and carbamidomethylation of cysteine was set as fixed modification. The precursor mass tolerance threshold was set 10 ppm for and maximum fragment mass error was 0.02 Da. The significance threshold of the ion score was calculated based on a false discovery rate of ≤1%. Qualitative analysis was performed using progenesis QI proteomics 4.1 (Nonlinear Dynamics).

Differential proteomic and pathway enrichment analyses

Proteins identified by mass spectrometry were quantified to identify differentially expressed proteins

between each experimental and control condition. ANOVA *P* value and absolute fold changes were used to identify differentially expressed proteins between wild-type and gene knockout mice. A protein was considered to be differentially expressed if the *P* value was ≤0.05 and the absolute fold change is ≥1.5. Gene enrichment analysis of differentially regulated proteins to identify known functions, pathways, and networks affected were performed using Ingenuity Pathway Analysis (IPA) (Ingenuity Systems; Mountain View, CA, USA) and Cytoscape used in conjunction with the plug-in Clue GO (Shannon *et al*. 2003; Bindea *et al*. 2009). False discovery rate for pathway analysis was controlled using the Benjamini–Hochberg procedure (Benjamini & Hochberg, 1995). Network representations of enriched pathways and gene ontology (GO) terms associated with biological process, molecular function, and KEGG pathways are graphically represented.

Statistical analyses

Physiological, biochemical and western blot data. Data are expressed as means ± SD. A *t* test was used for analysing the differences between gene knockout mice and wild-types using SigmaPlot software. A *P* value of < 0.05 was taken as indicative of statistical significance.

Proteomic and bioinformatic analyses. For all comparisons, ANOVA *P* value (computed from the proteomics core) was used. The cut-off used for Venn diagrams and general differential expression analysis summary was: *P* ≤ 0.05 and absolute fold change ≥1.5. IPA was also performed on genes with the same cut-off. For Volcano plots, the cut off used to add gene names to differentially expressed proteins were: absolute Log2fold change >1 and ANOVA *P* value ≤0.05.

Results

Characterization of Nrf2-associated genes and proteins in iMS-*Nrf2$^{flox/flox}$* and iMS-*Keap1$^{flox/flox}$* mice

Gene and protein expression data are shown in Fig. 1. The genotypes of mice were determined by PCR using genomic DNA isolated from tail snips that are shown in panel *A*. Subpanels (a) and (b) show the first generation of crossing HSA-MCM mice (human *α*-skeletal actin promoter-driven, mutated oestrogen receptor-controlled Cre) with Nrf2$^{flox/flox}$ or Keap1$^{flox/flox}$ mice where mice 1, 2,3 and 5 are *Cre$^{+/−}$;Nrf2$^{+/flox}$;*4 is *Cre$^{−/−}$;Nrf2$^{+/flox}$*; 11, 12, 13 and 15 are *Cre$^{−/−}$;Keap1$^{+/flox}$*; and 14 is *Cre$^{+/−}$;Keap1$^{+/flox}$*. Back breeding mice 1 and 14 (male) to female *Nrf2$^{flox/flox}$* or *Keap1$^{flox/flox}$* mice produced the second generation whose genotypes are shown in subpanels (c) and (d) where mice 6 and 7 are *Cre$^{−/−}$;Nrf2$^{+/flox}$;*8 and 10 are *Cre$^{+/−}$;Nrf2$^{flox/flox}$;* 9 is *Cre$^{−/−}$;Nrf2$^{flox/flox}$*; 16 is *Cre$^{+/−}$;Keap1$^{+/flox}$*; 17 and 20 are *Cre$^{+/−}$;Keap1$^{flox/flox}$*; 18 is

$Cre^{-/-};Keap1^{+/flox}$; and 19 is $Cre^{-/-};Keap1^{flox/flox}$. Mice 8, 10, 17 and 20 were the first generation of the inducible skeletal muscle-specific $Nrf2^{flox/flox}$ mice (iMS-$Nrf2^{flox/flox}$) or $Keap1^{flox/flox}$ mice (iMS-$Keap1^{flox/flox}$), which were the founders of all animals used in this study.

Fig. 1*B* shows PCR analyses of genomic DNA isolated from the Gas and liver of iMS-$Nrf2^{flox/flox}$ (subpanel (a)) or iMS-$Keap1^{flox/flox}$ (subpanel (b)) mice treated with Veh or Tamoxifen (Tam). The amplification of deleted $Nrf2$ allele at 467 bp and $Keap1$ allele at 288 bp were found selectively in Tam-treated Gas whereas the intact floxed $Nrf2$ allele at 2600 bp and $Keap1$ allele at 2954 bp presented in Veh-treated Gas and in both Tam- and Veh-treated livers provides evidence of silencing $Nrf2$ and $Keap1$ genes as reported previously (Kong *et al*. 2011), specifically in skeletal muscle in these models.

Fig. 1*C* shows the protein levels of Nrf2/Keap1 and targets in Sol and EDL of iMS-$Nrf2^{flox/flox}$ mice. We found that Nrf2, NQO1 and SOD2 were significantly lower in Tam-treated animals (KO) than the Veh-treated (WT), whereas Keap1, HO-1, SOD1, Cat and glutathione peroxidase (GPX) were not changed. Panel *D* shows these proteins in iMS-$Keap1^{flox/flox}$ mice. After Tam administration, Keap1 was significantly decreased, whereas Nrf2, NQO1, HO-1 and SOD2 were upregulated in both Sol and EDL compared with the Veh-treated group. Keap1 KO significantly upregulated catalase (Cat) only in Sol but not in EDL. In both muscles, the increase in SOD1 did not reach statistical significance whereas GPX displayed a tendency to downregulate after $Keap1$ was deleted.

In the above western blots there remained a small number of Nrf2 or Keap1 proteins present in gene knockout samples. These proteins most likely originate from non-muscle components of the samples, such as vessels, nerves and connective tissues, since the animal models are muscle-selective. However, we do not think these trace amounts of Nrf2 and Keap1 alter the phenotype of skeletal muscle that is deficient in Nrf2 or Keap1. In addition, we did not find significant changes in body weight or muscle mass in both models at the age and gene-deficient timeline used in the present study (32 weeks old with 20 weeks gene KO).

Exercise capacity and skeletal muscle functional analyses

Compared with Veh-treated mice, Tam-treated iMS-$Nrf2^{flox/flox}$ mice displayed significantly reduced maximal running speed, distance and duration whereas these parameters were enhanced in Tam-treated iMS-$Keap1^{flox/flox}$ mice (Fig. 2*A*). Fig. 2*B* shows *in situ* muscle contraction evoked by electrical stimulation. Subpanel (a) is a representative time course profile of maximal force induced by tetanic stimulation, showing the decline of force with time in EDL and Gas in WT mice. This process represents muscle fatigue and was enhanced in EDL and Gas in Nrf2-deficient mice and was abolished in

Keap1 KO mice. Sol force of WT mice was not altered in this time window, whereas it declined in Nrf2-deficient mice. Representative traces and mean data of force induced by the last tetanic stimulus are presented in subpanels (b) and (c), which clearly show a reduced force generation in Nrf2-deficient mice and enhanced force in *Keap1* KO mice.

Proteomic analyses

Proteomic analyses were carried out in Sol and EDL muscles from six iMS-Nrf2*flox/flox* mice and six iMS-*Keap1flox/flox* mice receiving either Veh or Tam. The muscle samples were assigned to eight groups (n = 3/group) and four comparison pairs: Nrf2-WT-Sol *vs*. Nrf2-KO-Sol, Nrf2-WT-EDL *vs*. Nrf2-KO-EDL, Keap1-WT-Sol *vs*. Keap1-KO-Sol, and Keap1-WT-EDL *vs*. Keap1-KO-EDL. We identified and quantified more than 1000 proteins for each sample, among which approximately 10% of proteins were significantly differentially expressed at a P value of 0.05. In Fig. 3, Volcano plots show the entire data set highlighting the proteins whose expression was significantly down- regulated (green) or upregulated (red) in gene KO muscle samples as compared with WT controls. The Venn diagram shows the number of proteins screened in each pair and the overlap between the comparisons. In total, we identified 114 proteins in Nrf2-deficient muscle (Table 1) and 117 proteins in Keap1-deficient muscle (Table 2), suggesting that these proteins can be assigned to two distinguishable categories. One group identified in Keap1-KO muscle is responsible for the well-known effects of Nrf2, such as antioxidant enzyme protein expression and detoxification, as shown in Fig. 4 and Fig. 5*B* in the following bioinformatics data. Most proteins in this group (108 of 117) were upregulated when *Keap1* was deleted. Accordingly, they are inducible in response to oxidative stress through a Keap1-dependent mechanism. The other group was identified in *Nrf2*-KO muscle. This group of proteins may mediate a novel function of Nrf2 that remains to be recognized. The expression of most proteins in this group (103 of 114) rely on basal Nrf2 activity since their abundance was significantly reduced when *Nrf2* was deleted. However, this group of proteins is independent of a Keap1 mechanism since we did not find differential expression of these proteins in *Keap1*-KO muscle. Please see the full list of proteins in these two groups in Tables 1 and 2. In this experiment, we found 10 proteins in common in the two groups, which are listed in Fig. 3*B*. These proteins were down- or upregulated, respectively, when *Nrf2* or *Keap1* was deleted, suggesting that their expressions are regulated by both basal Nrf2 activity and the Nrf2 released from its association with Keap1. One exception is Coq7 whose expression was increased in *Nrf2*- and *Keap1*-KO muscle. Interestingly, we observed that several sarcomeric proteins and contractile regulatory proteins were significantly altered in Nrf2- or Keap1-deficient

muscles. These skeletal muscle proteins are graphically represented in Fig. 3*C*.

Bioinformatic analyses

Gene ontology analyses. We employed GO analyses to functionally catalogue the identified proteins. Among the 114 proteins altered by deletion of *Nrf2*, 22.7% are involved in oxidoreduction coenzyme metabolism, 22.7% are purine ribonucleoside triphosphate metabolism, 13.6% are ATP metabolism, and 9.1% are propanoate metabolism, with the remaining 31.9% belonging to other pathways (Fig. 4*A*). Among the 117 proteins altered by deleting Keap1, 27.5% are cellular detoxification, 20% are NADP metabolism, 12.5% are glutathione metabolism, and 10.0% are electron transport chain proteins, while the remaining 30.0% belong to other pathways (Fig. 4*B*). Panels *C* and *D* show the biological processes of each function indicated in the pie charts. As we indicated above, the proteins identified in *Keap1* KO muscle contribute to the well-known Nrf2 effects, including detoxification, redox homeostasis, glutathione metabolism, and others, as shown in Panels *B* and *D*. The proteins identified in *Nrf2* KO muscle are involved in the processes such as coenzyme biosynthesis, glycolysis/gluconeogenesis, cellular senescence, propanoate metabolism, and others, as shown in Panels *A* and *C*. The implication of these biological processes in the Nrf2 effects remains to be elucidated.

Canonical pathways. Canonical pathway analysis was used to determine whether *Nrf2*- or *Keap1*-deletion altered the activity of intracellular pathways. We found that four pathways were activated in *Keap1*-deficient muscle. These are shown in Fig. 5*A*. Panel *B* indicates the specific protein components of each pathway that were upregulated when *Keap1* was deleted. For example, *Keap1*-KO activated Nrf2-mediated oxidative stress response by upregulating HSPs20/40/90, GSTs, NQO1, EPHX1, GCLC, CBR1, AOX1, CAT, SODs, TXN, GSR and TRXR1 (Fig. 5*B(1)*). The other three pathways activated were glutathione redox reactions I, glutathione-mediated detoxification, and the apelin adipocyte signalling pathway where the GST, GPX1, GSR, GPX and CAT were significantly upregulated when *Keap1* was deleted. Again, the proteins identified in *Keap1*-KO muscle contribute to well-recognized Nrf2 functions. In contrast, in the Nrf2-deficient muscle, we did not find any pathways that were altered, either positively or negatively, suggesting that the signalling pathway implication of the proteins downregulated when *Nrf2* was deleted remains to be elucidated.

Crosstalk of Nrf2 with other vital proteins. We employed IPA to look for key signalling proteins associated with the proteins identified in *Nrf2*- or *Keap1*-KO muscle. We found that 14 proteins were downregulated in *Nrf2* KO muscle and 12 proteins were upregulated in *Keap1* KO muscle that are either the downstream targets or upstream

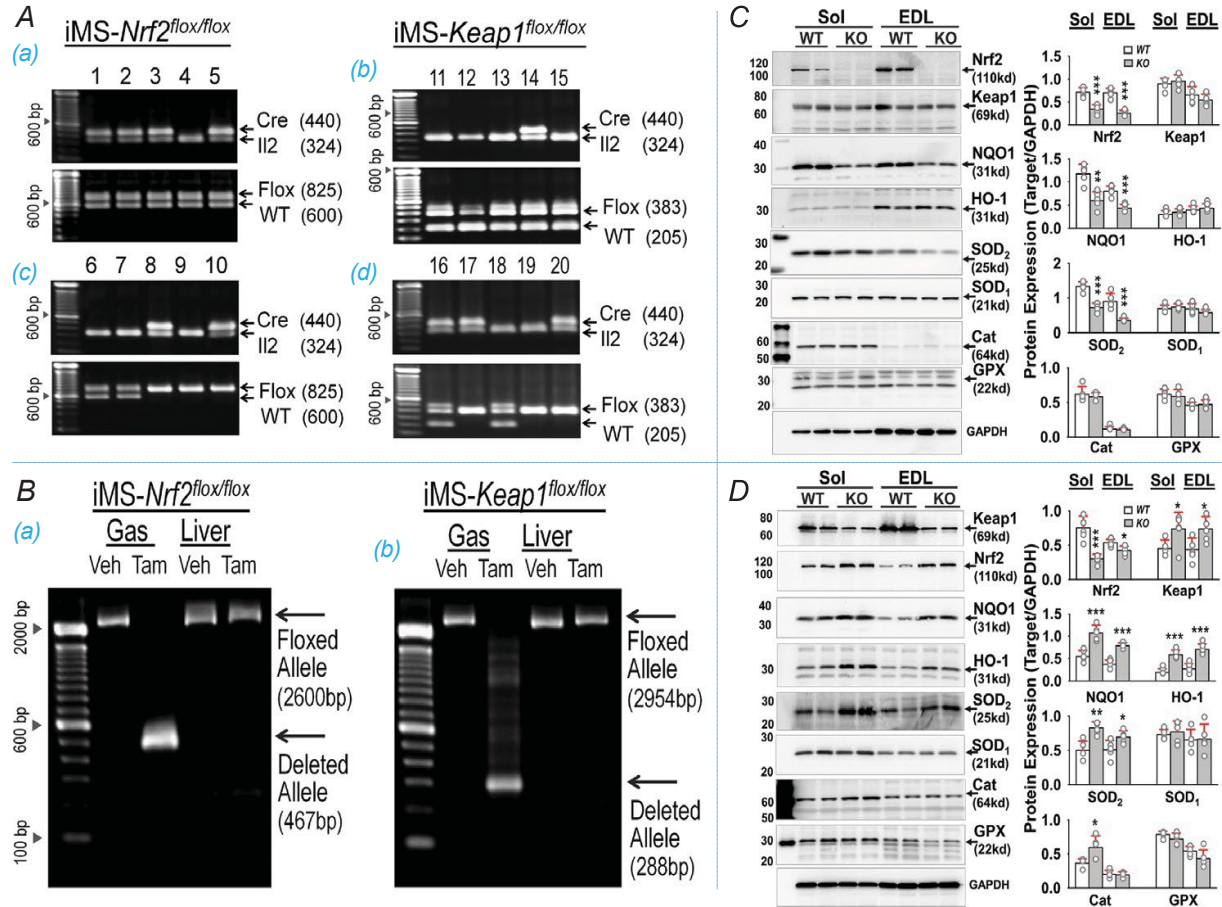regulators of P53, suggesting a crosstalk between Nrf2 and P53 (Fig. 6).

Figure 1. Gene and protein characterization of iMS-*Nrf2flox/flox* and iMS-*Keap1flox/flox* mice
A, genotypes of first (a and c) and second (b and d) generation mice to examine Cre, Floxed-Nrf2 and Floxed-Keap1 alleles. Il2: Interleukin-2 for internal control; WT: wild type. Mice 8 and 10 are iMS-*Nrf2flox/flox*. Mice 17 and 20 are iMS-*Keap1flox/flox*. *B*, PCR analysis of genomic DNA from the Gas muscle and liver of iMS-*Nrf2flox/flox* or iMS-*Keap1flox/flox* mice revealed amplification of intact flowed allele (2600 bp and 2954 bp) and deleted allele segments (467 bp and 288 bp). *C*, western blotting analyses of Nrf2, Keap1, NQO1, HO-1, SOD2, SOD, Cat and GPX in the soleus (Sol) and extensor digitorum longus (EDL) of iMS-*Nrf2flox/flox* mice received Veh (WT) or Tam (knockout, KO). Data are shown as the mean ± SD, with individual data points (n = 5). **P < 0.01, ***P < 0.001, KO *vs*. WT with unpaired t test by SigmaPlot software. *D*, western blotting analyses of Nrf2/Keap1 and downstream target proteins in Sol and EDL of iMS-*Keap1flox/flox* mice received Veh (WT) or Tam (KO). Data are shown as the mean ± SD, with individual data points (n = 5). *P < 0.05, **P < 0.01, ***P < 0.001, KO *vs*. WT with unpaired t test by SigmaPlot software. [Colour figure can be viewed at wileyonlinelibrary.com]

Pathological and physiological alterations. The IPA was also used to predict the functional alteration evoked by the proteins identified in *Nrf2*- or *Keap1*-KO muscle. Fig. 7*A* shows the muscle pathological events due to *Nrf2* KO-induced protein downregulation may include PFKM and HADHA-induced degeneration of muscle cells, NDUFS6-induced mitochondrial complex I deficiency of muscle, DNM1L-induced

muscular atrophy, HRAS-induced arrest in cell cycle progression of muscle cell lines, PRMT1 and EEF1A2-induced apoptosis of muscle cell lines, ARNTL, CST3, Pzp, ACADL, HSPA5 and FITM2-induced abnormal metabolism, and others. In contrast, several functions were enhanced due to Keap1 KO-induced protein upregulation, as shown in Fig. 7B, including CAT and NQO1-enhanced metabolism of ROS. Enhanced functions are contractility of muscle by upregulated NOL3, SYNC and XIRP1, the formation of muscle cells by upregulated CASQ1, AFG3L2 and XIRP1, and others. In addition, Nrf2 KO-impaired mitochondria, such as mitochondrial complex I deficiency, morphogenesis of mitochondria, abnormal morphology of mitochondria, permeability transition of mitochondria, dysfunction of mitochondria, transmembrane potential of mitochondria and the elongation, coupling, length and volume of mitochondria. These mitochondrial dysfunctions may be attributed to Nrf2 KO-induced downregulation of NDUFS6, PPID, PHB, YWHAE, DNM1L and AK1 (see Fig. 8)
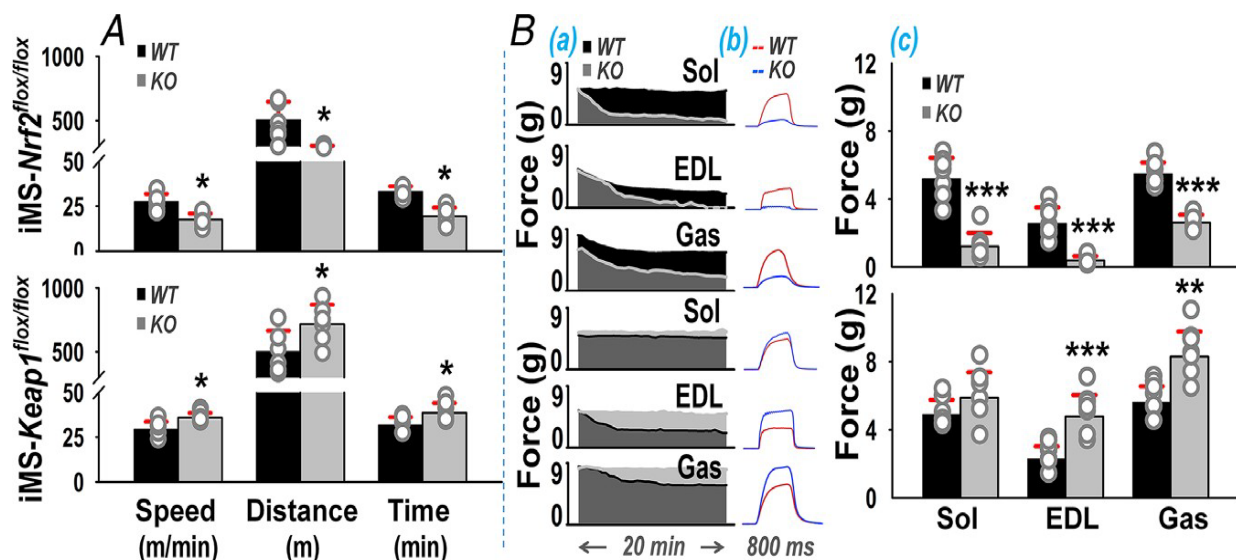

Figure 2. Functional alterations following gene deletion

A, treadmill running tests show reduced or enhanced exercise performance of *Nrf2*- or *Keap1*-KO mice. Data are shown as the mean ± SD, with individual data points ($n = 6$). *$P < 0.05$, knockout (KO) *vs*. wild-type (WT) with unpaired *t* test by SigmaPlot software. *B*, *in situ* functional tests show impaired or improved contractility of skeletal muscle deficient of Nrf2 or Keap1. (a) Representative time course profiles of maximal contractile response.

(b) Representative tracings of force generated by the last tetanus. (c) Mean data of force generated by the last tetanus, showing as the mean ± SD ($n = 7$). *$P < 0.05$, **$P < 0.01$, ***$P < 0.001$ KO *vs*. WT with unpaired *t* test by SigmaPlot software. [Colour figure can be viewed at wileyonlinelibrary.com]
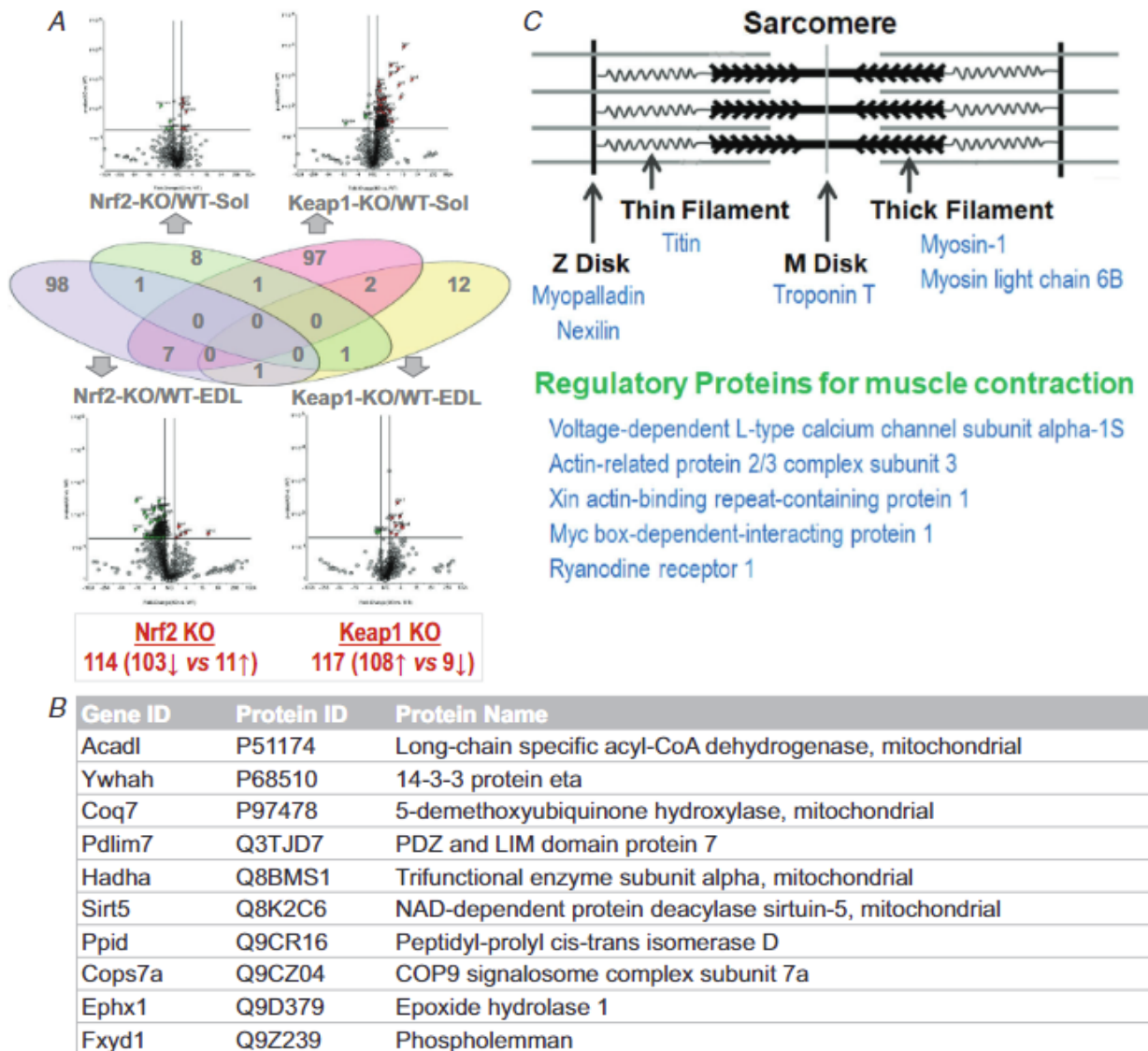
Figure 3. Mass spectrometry-based differential proteomic analysis of Nrf2- or Keap1-deficient skeletal muscle
A, Venn diagram showing overlap in quantified protein between the two muscle groups with or without Nrf2 or Keap1 deficiency. Volcano plots showing the fold change (knockout/wild-type) plotted against the *P* value highlighting significantly changed proteins (red – upregulation and green – downregulation; *P* :::; 0.05 and an absolute fold change of 1.5, *n* = 3, moderated *t* test). The vertical lines correspond to the absolute fold change of 1.5, and the horizontal line represents a *P* value of 0.05. *B*, 10 common proteins identified in *Nrf2*- and *Keap1*-KO muscle. *C*, schematic elucidation showing the sarcomere proteins and contractile regulatory proteins that were identified by mass spectrometry to be changed in Nrf2- or Keap1-deficient muscles.

Nrf2/Keap1 regulation of the glutaredoxin system. In addition to antioxidant mechanisms mediated by a panel of antioxidant enzymes, the proteomic and bioinformatic data reveal that the expression of several key proteins involved in the glutaredoxin system and thioredoxin system were altered when Nrf2 or Keap1 were deleted, suggesting that Nrf2/Keap1 also regulate these two anti- oxidant systems. Fig. 9A is a graphical representation of the glutaredoxin system-associated proteins identified in Nrf2- and Keap1-deficient muscle. Western blotting confirmed that glutathione reductase (GR),

thioredoxin reductase 1 (TrxR1), glutathione S-transferases alpha 2 (GSTA2), and glutathione S-transferases alpha 4 (GSTA4) were significantly downregulated in Nrf2-deficient muscles and upregulated in Keap1-deficient muscles, with the largest change in Sol when Keap1 was deleted (Fig. 9B). Fig. 9C shows the contents of glutathione in skeletal muscle, plasma and brain. GSH was significantly reduced or elevated in the muscle and plasma of the mice with muscle Nrf2 or Keap1 deficiency, but not in the brain.

Table 1. Differentially expressed proteins in Nrf2-deficient skeletal muscle				
Gene ID	**Protein ID**	**Protein name**	***P* value**	**Fold**
		***Nrf2* KO downregulated 103 proteins**		
Arntl	Q9WTL8	Aryl hydrocarbon receptor nuclear translocator – like protein 1	0.003	16.56
Tnnt3	Q9QZ47	Troponin T, fast skeletal muscle	0.004	2.51
Tuba1b	P05213	Tubulin alpha-1B chain	0.006	2.11
Surf4	Q64310	Surfeit locus protein 4	0.006	2.42
Usp47	Q8BY87	Ubiquitin carboxyl-terminal hydrolase 47	0.006	1.9
Pgm2l1	Q8CAA7	Glucose 1,6-bisphosphate synthase	0.006	3.65
Bckdha	P50136	2-oxoisovalerate dehydrogenase subunit alpha, mitochondrial	0.007	3.81
Nmnat3	Q99JR6	Nicotinamide/nicotinic acid mononucleotide adenylyltransferase 3	0.008	8.85
Stxbp3	Q60770	Syntaxin-binding protein 3	0.009	1.56
Dnm1l	Q8K1M6	Dynamin-1-like protein	0.01	2.59
Ndufb9	Q9CQJ8	NADH dehydrogenase (ubiquinone) 1 beta subcomplex subunit 9	0.01	8.59
Prmt1	Q9JIF0	Protein arginine N-methyltransferase 1	0.01	1.62
Kif1a	P33173	Kinesin-like protein KIF1A	0.01	2.76
Tsnax	Q9QZE7	Translin-associated protein X	0.01	2.4
Crkl	P47941	Crk-like protein OS = Mus musculus OX = 10,090 GN = Crkl PE = 1 SV = 2	0.01	3.91
Acadl	P51174	Long-chain specific acyl-CoA dehydrogenase, mitochondrial	0.02	3.53
Gstm1	P10649	Glutathione S-transferase Mu 1	0.02	1.98
Tuba8	Q9JJZ2	Tubulin alpha-8 chain	0.02	2.36
Glud1	P26443	Glutamate dehydrogenase 1, mitochondrial	0.02	1.9
Rtn2	O70622	Reticulon-2	0.02	2.04
Rpn1	Q91YQ5	Dolichyl-diphosphooligosaccharide–protein glycosyltransferase subunit 1	0.02	2.21
Cbr1	P48758	Carbonyl reductase (NADPH) 1	0.02	2.2
Pdlim7	Q3TJD7	PDZ and LIM domain protein 7	0.02	2.73
Pdpr	Q7TSQ8	Pyruvate dehydrogenase phosphatase regulatory subunit, mitochondrial	0.02	2.06
Psmd11	Q8BG32	26S proteasome non-ATPase regulatory subunit 11	0.02	2.79
Myl4	P09541	Myosin light chain 4	0.02	5.58
Rbm3	O89086	RNA-binding protein 3	0.02	3.15
Nlrx1	Q3TL44	NLR family member X1	0.02	2.6
Fxyd1	Q9Z239	Phospholemman	0.02	2.64
Bola1	Q9D8S9	BolA-like protein 1	0.02	2.64
				continued next page

Rpl15	Q9CZM2	60S ribosomal protein L15	0.02	2.52
Hddc2	Q3SXD3	HD domain-containing protein 2	0.02	2.28
Smc3	Q9CW03	Structural maintenance of chromosomes protein 3	0.02	3.4
HRAS	Q61411	GTPase HRas	0.02	2.51
Hadha	Q8BMS1	Trifunctional enzyme subunit alpha, mitochondrial	0.03	1.89
Hspa5	P20029	Endoplasmic reticulum chaperone BiP	0.03	2.92
Dld	O08749	Dihydrolipoyl dehydrogenase, mitochondrial	0.03	3.26
Padi2	Q08642	Protein arginine deiminase type-2	0.03	2.88
Ca3	P16015	Carbonic anhydrase 3	0.03	4.26
Ldhb	P16125	L-lactate dehydrogenase B chain	0.03	3.04
Synpo2l	Q8BWB1	Synaptopodin 2-like protein OS = Mus musculus	0.03	3.5
Tmed10	Q9D1D4	Transmembrane emp24 domain-containing protein 10	0.03	3.71
Nap1l4	Q78ZA7	Nucleosome assembly protein 1-like 4	0.03	1.83
Acsl6	Q91WC3	Long-chain-fatty-acid–CoA ligase 6	0.03	3.46
Ddost	O54734	Dolichyl-diphosphooligosaccharide–protein glycosyltransferase 48 kDa subunit	0.03	3.8
Psma5	Q9Z2U1	Proteasome subunit alpha type-5	0.03	2.26
Eif4h	Q9WUK2	Eukaryotic translation initiation factor 4H	0.03	3.39
Apmap	Q9D7N9	Adipocyte plasma membrane-associated protein	0.03	2.16
Rpl24	Q8BP67	60S ribosomal protein L24 OS = Mus musculus	0.03	2.31
Hmgcl	P38060	Hydroxymethylglutaryl-CoA lyase, mitochondrial	0.03	24.29
Prkag1	O54950	Kinesin-like protein KIF1A	0.03	1.88
Psma2	P49722	Proteasome subunit alpha type-2	0.03	2.43
Sept7	O55131	Septin-7	0.03	142.77
Rax	O35602	Retinal homeobox protein Rx	0.03	1.95
Ak1	Q9R0Y5	Adenylate kinase isoenzyme 1	0.04	2.37
Idh3g	P70404	Isocitrate dehydrogenase (NAD) subunit gamma 1, mitochondrial	0.04	3.57
Vcl	Q64727	Vinculin	0.04	2.44
Pzp	Q61838	Pregnancy zone protein	0.04	2.35
Pdlim5	Q8CI51	PDZ and LIM domain protein 5	0.04	3.49
Spr	Q64105	Sepiapterin reductase	0.04	4.58
Acp1	Q9D358	Low molecular weight phosphotyrosine protein phosphatase	0.04	1.59
Ywhah	P68510	14-3-3 protein eta	0.04	3.76
Canx	P35564	Calnexin	0.04	2.79
Mylk	Q6PDN3	Myosin light chain kinase, smooth muscle	130.2	0.04
Aldoc	P05063	Fructose-bisphosphate aldolase C	0.04	5.7
Ppid	Q9CR16	Peptidyl-prolyl cis-trans isomerase D	0.04	2.45
Sumo3	Q9Z172	Small ubiquitin-related modifier 3	0.04	2.72
Cops7a	Q9CZ04	COP9 signalosome complex subunit 7a	0.04	2.14
Farsa	Q8C0C7	Phenylalanine–tRNA ligase alpha subunit	0.04	11.81
Fitm2	P59266	Fat storage-inducing transmembrane protein 2	0.04	24.95
Adprh	P54923	(Protein ADP-ribosylarginine) hydrolase	0.04	3.82
Thnsl2	Q80W22	Threonine synthase-like 2	0.04	9.85
PFKM	P47857	ATP-dependent 6-phosphofructokinase, muscle type	0.05	1.65
Aco2	Q99KI0	Aconitate hydratase, mitochondrial	0.05	2.35
Eef1a2	P62631	Elongation factor 1-alpha 2	0.05	2.75
Ndufa	Q99LC3	NADH dehydrogenase (ubiquinone) 1 alpha subcomplex subunit 10, mitochondrial	0.05	3.13
Ivd	Q9JHI5	Isovaleryl-CoA dehydrogenase, mitochondrial	0.05	2.71
Smyd1	P97443	Histone-lysine N-methyltransferase Smyd1	0.05	1.64
YWHAE	P62259	14-3-3 protein epsilon	0.05	2.31
PHB	P67778	Prohibitin	0.05	1.75

Selenbp1	P17563	Methanethiol oxidase	0.05	1.81
Capns1	O88456	Calpain small subunit 1	0.05	9.8
Rps27a	P62983	Ubiquitin-40S ribosomal protein S27a	0.05	2.21
Ndufs6	P52503	NADH dehydrogenase (ubiquinone) iron-sulfur protein 6, mitochondrial	0.05	3.23
Tkt	P40142	Transketolase	0.05	3.95
Cst3	P21460	Cystatin-C	0.05	4.12
Pfdn2	O70591	Prefoldin subunit 2	0.05	2.78
Gps1	Q99LD4	COP9 signalosome complex subunit 1	0.05	1.94
Nptn	P97300	Neuroplastin	0.05	2.81
Tmpo	Q61029	Lamina-associated polypeptide 2, isoforms beta/delta/epsilon/gamma	0.05	1.24
Anp32e	P97822	Acidic leucine-rich nuclear phosphoprotein 32 family member E	0.05	5.15
Ppp6c	Q9CQR6	Serine/threonine-protein phosphatase 6 catalytic subunit	0.05	3.43
Atox1	O08997	Copper transport protein ATOX1	0.05	3.41
Cstb	Q62426	Cystatin-B	0.05	2.72
Ruvbl2	Q9WTM5	RuvB-like 2	0.05	4.21
Farsb	Q9WUA2	Phenylalanine–tRNA ligase beta subunit	0.05	2.86
Ak2	Q9WTP6	Adenylate kinase 2, mitochondrial	0.05	2.26
Mars	Q68FL6	Methionine–tRNA ligase, cytoplasmic	0.05	86.53
Ptges3l	Q9D9A7	Putative protein PTGES3L	0.05	6.28
Sirt5	Q8K2C6	NAD-dependent protein deacylase sirtuin-5, mitochondrial	0.05	3.68
Ephx1	Q9D379	Epoxide hydrolase 1	0.04	1.71
Fermt2	Q8CIB5	Fermitin family homolog 2	0.05	2.1
N/A	P01864	Ig gamma-2A chain C region secreted form	0.05	2.74
Nrf2 KO upregulated 11 proteins				
Azgp1	Q64726	Zinc-alpha-2-glycoprotein	0.002	00
Pon2	Q62086	Serum paraoxonase/arylesterase 2	0.02	2.16
Pdxk	Q8K183	Pyridoxal kinase	0.03	3.9
Coq7	P97478	5-demethoxyubiquinone hydroxylase, mitochondrial	0.04	2.35
Akap1	O08715	A-kinase anchor protein 1, mitochondrial	0.05	1.84
Eif2s3x	Q9Z0N1	Eukaryotic translation initiation factor 2 subunit 3, X-linked	0.005	1.63
Mief2	Q5NCS9	Mitochondrial dynamics protein MID49	0.006	1.7
Hnrnpa3	Q8BG05	Heterogeneous nuclear ribonucleoprotein A3	0.008	1.56
Hist1h2ab	C0HKE1	Histone H2A type 1-B	0.01	2.31
Higd2a	Q9CQJ1	HIG1 domain family member 2A	0.05	1.96
Yars	Q91WQ3	Tyrosine–tRNA ligase, cytoplasmic	0.05	2.36

Mitochondria content and function. The IPA data suggest that Nrf2-deficient skeletal muscle exhibits multiple disorders associated with mitochondrial function (Fig. 8). Accordingly, we examined mitochondrial content and respiration of skeletal muscle after Nrf2 or Keap1 deficiency (Fig. 10).

Citrate synthase activity. We measured CS activity of Sol muscles to assess mitochondrial content. CS activity in *Nrf2*-KO muscle was significantly lower compared with *Nrf2*-WT, *Keap1*-KO and *Keap1*-WT (32 ± 3 *vs.* 50 ± 7, 51 ± 5, and 54 ± 3 nmol min^{-1} μg^{-1} protein; Fig. 10*A*).

Mitochondrial respiratory complex protein expression. Fig. 10*B* shows western

blot data of mitochondrial respiratory complex protein expression from skeletal muscle following the deletion of *Nrf2* or *Keap1*. We found that *Nrf2* KO muscle resulted in significant down- regulation of all five respiratory chain complexes in the EDL and three complexes (I, III and IV) in the Sol. *Keap1* KO muscle tended to exhibit upregulation of these complexes but did not reach statistical significance.

Mitochondrial respiratory complex function. Skeletal muscle mitochondrial respiration was assessed in both Sol and EDL. In the Sol, mitochondrial complex I state 2 respiration, i.e. uncoupled respiration, was significantly higher in Nrf2-KO vs. Nrf2-WT (28 ± 15 vs. 18 ± 8 pmol mg−1 wet weight s−1) (Fig. 10C(a)). However, complex I state 3 and complex I+II state 3 respiration, coupled respiration, were significantly lower in Nrf2-KO vs. Nrf2-WT (24 ± 17 vs. 32 ± 6; 31 ± 18 vs. 54 ± 8 pmol mg−1 wet weight s−1) (Fig. 10C(a)). Interestingly, there were no differences in both uncoupled and coupled respiration between Keap1-WT and Keap1-KO (Fig. 10C(b)). In addition, when we compared mitochondrial respiration between Nrf2-KO and Keap1-KO, we found that Nrf2-KO exhibited greater state 2 (uncoupled) respiration (28 ± 15 vs. 17 ± 3 pmol mg−1 wet weight s−1, $p < 0.05$) but lower complex I state 3 and complex I+II state 3 (coupled) respiration (24 ± 17 vs. 31 ± 6; 31 ± 18 vs. 50 ± 2 pmol mg−1 wet weight s−1, $p < 0.05$) compared with Keap1-KO (Fig. 10C(c)). Furthermore, complex IV respiration, uncoupled mediated maximum oxygen consumption capacity, was lower in Nrf2-KO than Nrf2-WT (161 ± 72 vs. 237 ± 84 pmol mg−1 wet weight s−1) and Keap1-KO (161 ± 72 vs. 245 ± 8 pmol mg−1 wet weight s−1). Mitochondrial respiration in EDL showed similar trends compared with those from Sol; however, measures of mitochondrial respiration in EDL were not statistically significant (Fig. 10D(a),(b),(c)).

Table 2. Differentially expressed proteins in Keap1-deficient skeletal muscle				
Gene ID	**Protein ID**	**Protein name**	***P* value**	**Fold**
Keap1 KO upregulated 108 proteins				
Nqo1	Q64669	NAD(P)H dehydrogenase (quinone) 1	0.0001	17.47
Gsta4	P24472	Glutathione S-transferase A4	0.0004	5.24
Q9D975	P10648	Glutathione S-transferase A2	0.0006	10.24
Gbe1	Q9D6Y9	1,4-alpha-glucan-branching enzyme	0.0009	5.03
			continued next page	
Srxn1	Q9D975	Sulfiredoxin-1	0.0013	33.94
Phkb	Q7TSH2	Phosphorylase b kinase regulatory subunit beta	0.0015	1.7
Cbr3	Q8K354	Carbonyl reductase (NADPH) 3	0.0019	11.66
Tsn	Q62348	Translin	0.0021	1.58
Cpt2	P52825	Carnitine O-palmitoyltransferase 2, mitochondrial	0.0021	1.82
PPID	Q9CR16	Peptidyl-prolyl cis-trans isomerase D	0.0028	1.41
Prdx6	O08709	Peroxiredoxin-6	0.0029	1.9
			continued next page	

Arl6ip5	Q8R5J9	PRA1 family protein 3	0.0046	1.53
Pir	Q9D711	Pirin	0.0048	11.29
Txnrd1	Q9JMH6	Thioredoxin reductase 1, cytoplasmic	0.0052	3.2
Cat	P24270	Catalase	0.0056	2.34
Nol3	Q9D1 × 0	Nucleolar protein 3	0.0057	2.29
Coq4	Q8BGB8	Ubiquinone biosynthesis protein COQ4 homolog, mitochondrial	0.0058	1.75
Coq7	P97478	5-demethoxyubiquinone hydroxylase, mitochondrial	0.006	2.02
Ndufb10	Q9DCS9	NADH dehydrogenase (ubiquinone) 1 beta subcomplex subunit 10	0.0068	1.28
Atp2b1	G5E829	Plasma membrane calcium-transporting ATPase 1	0.0084	1.76
Gclc	P97494	Glutamate–cysteine ligase catalytic subunit	0.0085	2.14
Coq3	Q8BMS4	Ubiquinone biosynthesis	0.0097	1.74
Uba1	Q02053	Ubiquitin-like modifier-activating enzyme 1	0.01	1.29
Tuba4a	P68368	Tubulin alpha-4A chain	0.01	1.57
Taldo1	Q93092	Transaldolase	0.01	4.04
Gstm2	P15626	Glutathione S-transferase Mu 2	0.01	1.9
Gsr	P47791	Glutathione reductase, mitochondrial	0.01	4.72
Acss1	Q99NB1	Acetyl-coenzyme A synthetase 2-like, mitochondrial	0.01	2.31
Psmb1	O09061	Proteasome subunit beta type-1	0.01	1.37
Ank3	G5E8K5	Ankyrin-3	0.01	2.66
Nek7	Q9ES74	Serine/threonine-protein kinase Nek7	0.01	2.05
Tango2	P54797	Transport and Golgi organization 2 homolog	0.01	1.24
Sirt5	Q8K2C6	NAD-dependent protein deacylase sirtuin-5, mitochondrial	0.01	1.39
Hmox2	O70252	Heme oxygenase 2	0.01	2.06
Dusp13	Q6B8I0	Dual specificity protein phosphatase 13 isoform A	0.01	3.69
Acadl	P51174	Long-chain specific acyl-CoA dehydrogenase, mitochondrial	0.02	1.44
Aldh2	P47738	Aldehyde dehydrogenase, mitochondrial	0.02	2.1
Bin1	O08539	Myc box-dependent-interacting protein 1	0.02	1.53
Psmd5	Q8BJY1	26S proteasome non-ATPase regulatory subunit 5	0.02	2.9
Gstz1	Q9WVL0	Maleylacetoacetate isomerase	0.02	1.84
Esd	Q9R0P3	S-formylglutathione hydrolase	0.02	2.99
Krt10	P02535	Keratin, type I cytoskeletal 10	0.02	2.79
Uggt1	Q6P5E4	UDP-glucose:glycoprotein glucosyltransferase 1	0.02	1.63
Arpc3	Q9JM76	Actin-related protein 2/3 complex subunit 3	0.02	1.7
Glrx	Q9QUH0	Glutaredoxin-1	0.02	2.07
Stoml2	Q99JB2	Stomatin-like protein 2, mitochondrial	0.02	1.82
Atp5f1a	Q03265	ATP synthase subunit alpha, mitochondrial	0.03	1.58
Tufm	Q8BFR5	Elongation factor Tu, mitochondrial	0.03	1.66
Vwa8	Q8CC88	von Willebrand factor A domain-containing protein 8	0.03	1.75
Cycs	P62897	Cytochrome c, somatic	0.03	1.74
Ephx1	Q9D379	Epoxide hydrolase 1	0.03	4.24
Eprs	Q8CGC7	Bifunctional glutamate/proline–tRNA ligase	0.03	2.07
Pgd	Q9DCD0	6-phosphogluconate dehydrogenase, decarboxylating	0.03	2.08
Bzw2	Q91VK1	Basic leucine zipper and W2 domain-containing protein 2	0.03	1.89
Cops7a	Q9CZ04	COP9 signalosome complex subunit 7a	0.03	1.47
Pdlim7	Q3TJD7	PDZ and LIM domain protein 7	0.03	1.71
Me1	P06801	NADP-dependent malic enzyme	0.03	1.7
Coa3	Q9D2R6	Cytochrome c oxidase assembly factor 3 homolog, mitochondrial	0.03	1.49
Cyb5b	Q9CQX2	Cytochrome b5 type B	0.03	2.21
Prkag2	Q91WG5	5'-AMP-activated protein kinase subunit gamma-2	0.03	1.49

Aox1	O54754	Aldehyde oxidase 1	0.03	2.5
Homer2	Q9QWW1	Homer protein homolog 2	0.03	1.67
Cops8	Q8VBV7	COP9 signalosome complex subunit 8	0.03	1.66
Mup3	P04939	Major urinary protein 3	0.03	7.92
Hyou1	Q9JKR6	Hypoxia upregulated protein 1	0.03	1.75
Hadha	Q8BMS1	Trifunctional enzyme subunit alpha, mitochondrial	0.04	1.71
Ttn	A2ASS6	Titin	0.04	1.25
Ech1	O35459	Delta(3,5)-Delta(2,4)-dienoyl-CoA isomerase, mitochondrial	0.04	1.59
Hspb7	P35385	Heat shock protein beta-7	0.04	1.56
Slc27a1	Q60714	Long-chain fatty acid transport protein 1	0.04	1.57
Afg3l2	Q8JZQ2	AFG3-like protein 2	0.04	1.84
Gfm1	Q8K0D5	Elongation factor G, mitochondrial	0.04	1.41
Thtpa	Q8JZL3	Thiamine-triphosphatase	0.04	2.39
Fxyd1	Q9Z239	Phospholemman	0.04	1.53
Faf1	P54731	FAS-associated factor 1	0.04	1.64
Aspscr1	Q8VBT9	Tether containing UBX domain for GLUT4	0.04	1.66
Lars	Q8BMJ2	Leucine–tRNA ligase, cytoplasmic	0.04	1.85
Sync	Q9EPM5	Syncoilin	0.04	1.81
Emc4	Q9CZX9	ER membrane protein complex subunit 4	0.04	1.36
Mapk3	Q63844	Mitogen-activated protein kinase 3	0.04	1.44
Lmod3	E9QA62	Leiomodin-3	0.04	2.15
Timm8a2	Q4FZG7	Putative mitochondrial import inner membrane translocase subunit Tim8 A-B	0.04	2.06
Fam234a	Q8C0Z1	Protein FAM234A	0.04	1.92
Atp5f1b	P56480	ATP synthase subunit beta, mitochondrial	0.05	1.78
Casq1	O09165	Calsequestrin-1	0.05	1.84
Hibch	Q8QZS1	3-hydroxyisobutyryl-CoA hydrolase, mitochondrial	0.05	1.41
Ndufa5	Q9CPP6	NADH dehydrogenase (ubiquinone) 1 alpha subcomplex subunit 5	0.05	1.69
Mpc2	Q9D023	Mitochondrial pyruvate carrier 2	0.05	1.47
Mtx1	P47802	Metaxin-1	0.05	1.59
Rdh13	Q8CEE7	Retinol dehydrogenase 13	0.05	1.55
Mcu PE	Q3UMR5	Calcium uniporter protein, mitochondrial	0.05	2.01
Xirp1	O70373	Xin actin-binding repeat-containing protein 1	0.05	2.21
Rpl9	P51410	60S ribosomal protein L9	0.05	1.62
Sec23a	Q01405	Protein transport protein Sec23A	0.05	2.94
Trim16	Q99PP9	Tripartite motif-containing protein 16	0.05	1.8
Retreg1	Q8VE91	Reticulophagy regulator 1	0.05	2.3
Xirp2	Q4U4S6	Xin actin-binding repeat-containing protein 2	0.05	2.15
Rab11fip5	Q8R361	Rab11 family-interacting protein 5	0.05	1.99
Plec	Q9QXS1	Plectin	0.0005	1.4
N/A	P06330	Ig heavy chain V region AC38 205.12	0.01	3.96
Atp6v1a	P50516	V-type proton ATPase catalytic subunit A	0.01	1.84
Myoz2	Q9JJW5	Myozenin-2	0.02	2.55
Malsu1	Q9CWV0	Mitochondrial assembly of ribosomal large subunit protein 1	0.02	4.81
Hbb-b1	P02088	Haemoglobin subunit beta-1	0.04	1.62
Ywhah	P68510	14-3-3 protein eta	0.04	1.97
N/A	P01654	Ig kappa chain V-III region PC 2880/PC 1229	0.04	2.9
Psmd13	Q9WVJ2	26S proteasome non-ATPase regulatory subunit 13	0.05	1.6
Apoc1	P34928	Apolipoprotein C-I	0.05	7.17

Keap1 KO downregulated 9 proteins				
Lta4h	P24527	Leukotriene A-4 hydrolase	0.004	1.41
Gpd1	P13707	Glycerol-3-phosphate dehydrogenase (NAD^{+}), cytoplasmic	0.0097	1.56
Pcyt2	Q922E4	Ethanolamine-phosphate cytidylyltransferase	0.02	2.01
Serpinf1	P97298	Pigment epithelium-derived factor	0.02	1.19
Senp8	Q9D2Z4	Sentrin-specific protease 8	0.02	1.9
N/A	P01643	Ig kappa chain V-V region MOPC 173	0.03	20.49
Cacna1s	Q02789	Voltage-dependent L-type calcium channel subunit alpha-1S	0.05	1.57
Sh3bgr	Q9WUZ7	SH3 domain-binding glutamic acid-rich protein	0.03	1.64
Rps5	P97461	40S ribosomal protein S5	0.03	2.18

Discussion

Intracellular redox homeostasis is essential for skeletal myocytes to maintain normal structure, function, and metabolism (McDonagh, 2016; Mukund *et al*. 2019). Excessive ROS oxidize cellular proteins, lipids and DNA/RNA, contributing to skeletal muscle wasting, contractile dysfunction, early fatigue and metabolic disorders (Powers & Jackson, 2008; Powers *et al*. 2016). The *Nrf2*/*Keap1* complex is a pivotal transcriptional regulatory system that controls expression of a panel of anti- oxidant enzymes and many other cytoprotective proteins. Accumulating evidence documents a crucial role for a well-functioning Nrf2 system in normal skeletal muscle and contribution of an impaired *Nrf2*/*Keap1* signalling to skeletal myopathy in ageing (Ahn *et al*. 2018) and chronic diseases (Wafi *et al*. 2018). Moreover, Nrf2 has been suggested as a promising therapeutic target in several pathological conditions (Cuadrado *et al*. 2018, 2019). However, the precise biological implication of Nrf2 in skeletal muscle remains to be elucidated. In this study, we developed two mouse lines targeting skeletal muscle Nrf2, by employing which we tested the impact of *Nrf2*- or *Keap1*-deletion on exercise capacity and *in situ* muscle contractility. We also performed mass spectrometry and bioinformatics to analyse Nrf2- or Keap1-deficient skeletal muscle and to explore the frontier of Nrf2 function and downstream pathways. Finally, we chose the glutaredoxin system and mitochondria to confirm mass spectrometry results by examining glutathione metabolism-associated proteins and mitochondrial respiratory function.

By crossing HSA-MCM with Nrf2*flox/flox* or Keap1*flox/flox* mouse lines, we successfully generated two models, the iMS-*Nrf2flox/flox* and iMS-*Keap1flox/fox*, which allowed us to knock out skeletal muscle *Nrf2* or *Keap1* genes, subsequently down- or upregulating Nrf2 and its downstream signalling pathways. Genotyping showed that these mice carry both HSA-Cre and Nrf2*flox/flox* or Keap1*flox/flox* alleles (Fig. 1*A*), suggesting that the *Nrf2* or *Keap1* gene in skeletal myocytes can be deleted in an inducible manner. After administration of tamoxifen, we detected the deleted *Nrf2* or *Keap1*allele segments in Gas but not in the

liver (Fig. 1*B*), demonstrating skeletal muscle specificity in this genetic modification. Employing western blot analysis, we found a downregulation of Nrf2, NQO1 and SOD2 proteins in iMS-Nrf2*flox/flox* mice (Fig. 1*C*) and upregulation of Nrf2, NQO1, HO-1, and SOD2 proteins in iMS-Keap1*flox/flox* mice (Fig. 1*D*), suggesting an extreme change in Nrf2 downstream signalling. We further found that exercise capacity and muscle tolerance to fatigue were significantly reduced in iMS-Nrf2*flox/flox* but increased in iMS-Keap1*flox/flox* mice (Fig. 2), suggesting a profound impact of Nrf2 on skeletal muscle function.
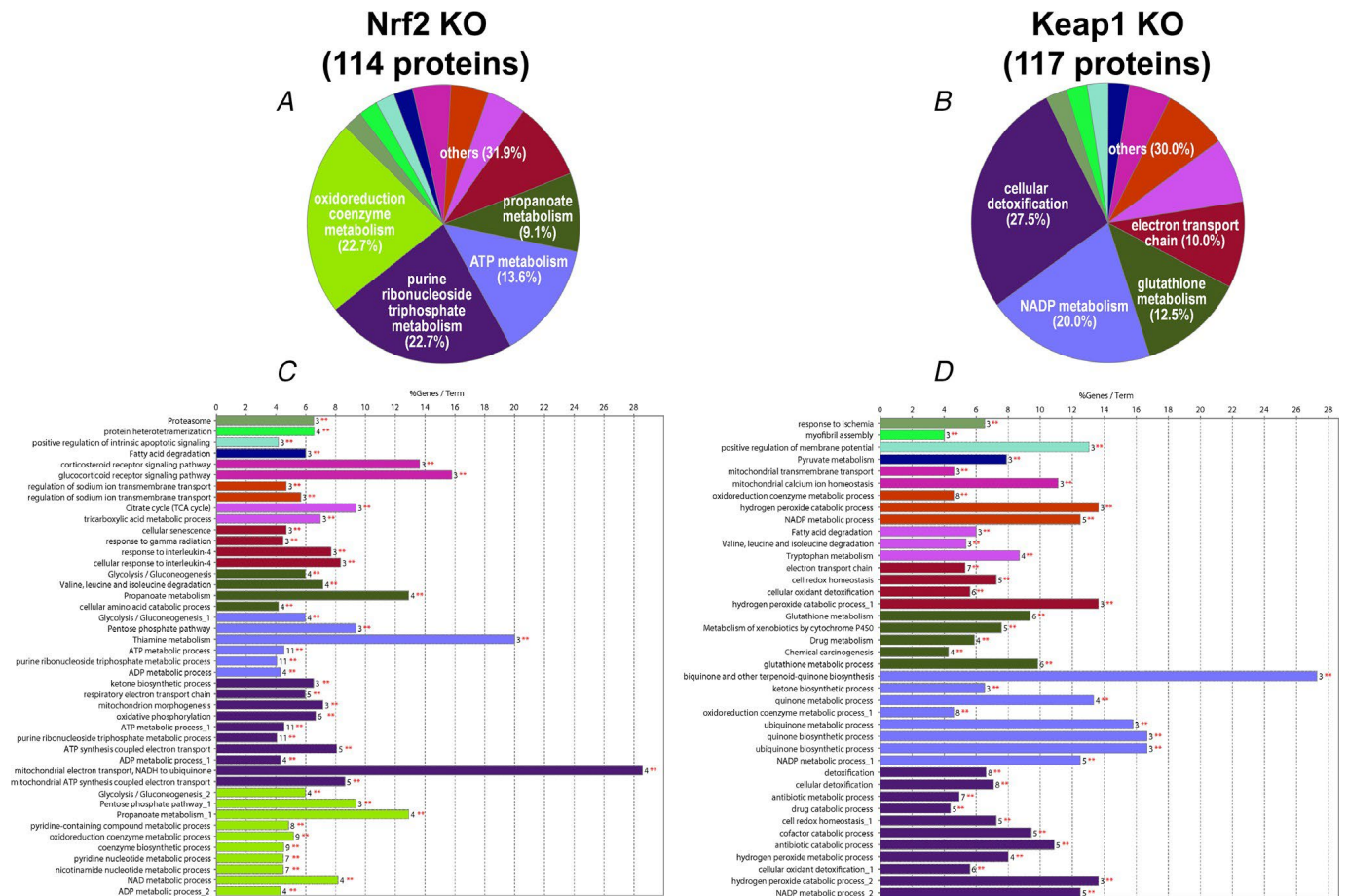
Figure 4. Functional catalogues of the proteins identified in Nrf2- (*A* & *C*) or Keap1- (*B* & *C*) deficient muscle

A, B, pie charts representing the distribution of identified differentially expressed proteins according to their biological process; *C, D*, bar charts demonstrating the specific processes that correspond to the classification. The same colour key that was used in the pie charts has also been applied in these charts.
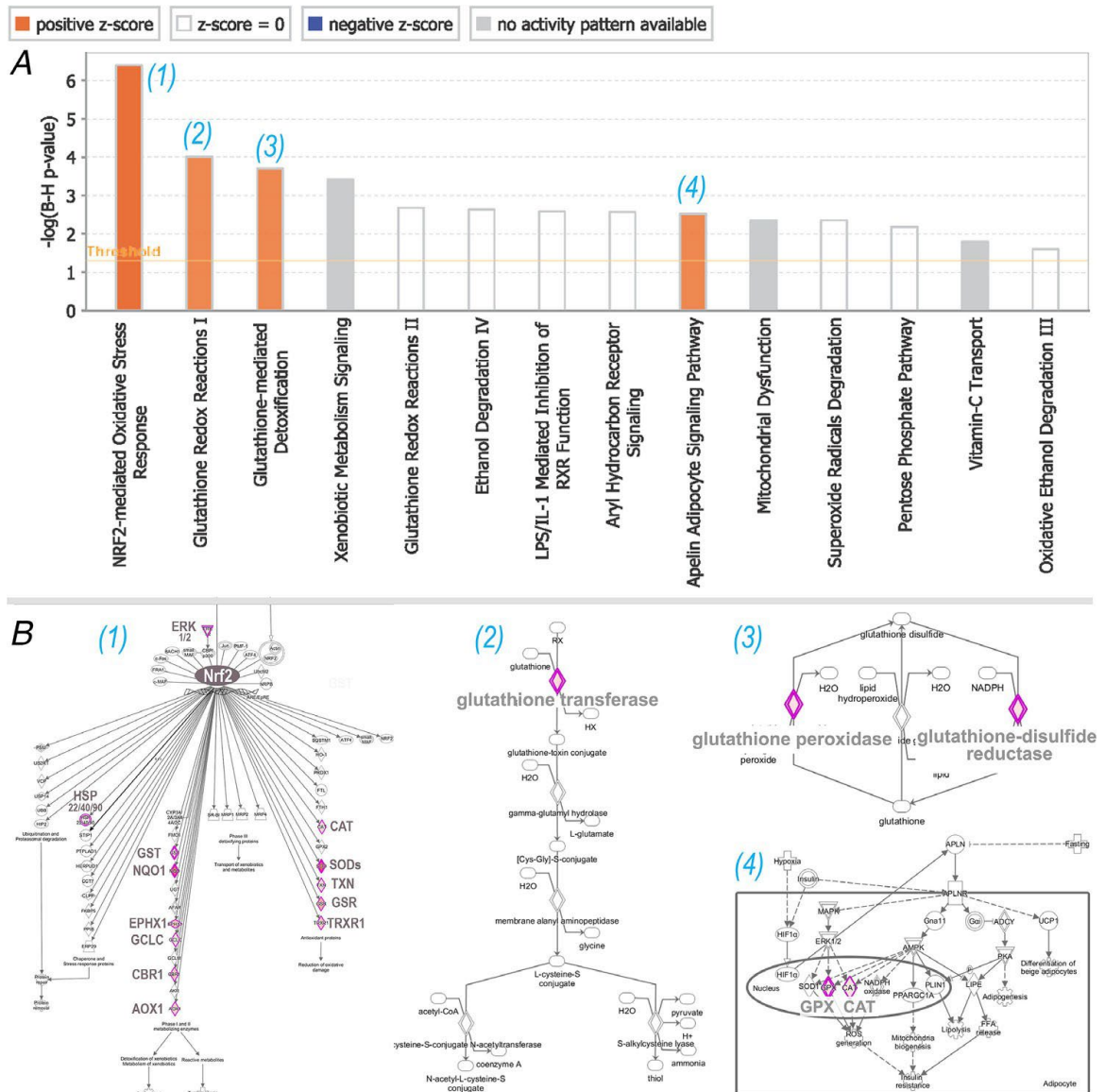
Figure 5. Canonical pathways activated in Keap1-KO muscle
A, Benjamini–Hochberg false discovery rate corrected pathways differentially expressed in Keap1-KO muscle. The x-axis represents the pathways identified and the y-axis shows the –log of the value calculated based on Fisher's exact test with multiple corrections. Orange bars indicate the pathways activated. B, proteins upregulated by Keap1-KO (red rhombus) corresponded to the specific components of each pathway.

In the proteomics data, we found that *Nrf2* KO changed 114 proteins, 103 of which were downregulated. On the other hand, *Keap1* KO resulted in 117 differentially expressed proteins with 108 being upregulated (Fig. 3*A*). Interestingly, among these proteins only 10 were in common, strongly suggesting that the proteins identified in *Nrf2-* and *Keap1*-KO muscle can be assigned to two categories, which are responsible for different *Nrf2* functions. Indeed, as suggested by bioinformatic analysis, *Keap1* KO-upregulated proteins evoke the well-known Nrf2 effects, such as antioxidant

defence and detoxification. However, the precise significance of the proteins downregulated by

Nrf2 KO remains to be elucidated. In addition, mass spectrometry data revealed that several sarcomeric

proteins and contractile regulatory proteins were differentially expressed. Titin, the largest protein responsible

for passive elasticity of muscle (Granzier *et al*. 2000), was significantly upregulated when *Keap1* was

deleted, whereas Troponin T, a protein responsible for transducing Ca^{2+} signals in the regulation of

contraction (Mondal & Jin, 2016), was downregulated in Nrf2-deficient muscles (Fig. 3*C*). These

changes represent potential mechanisms underlying the functional alteration observed previously and

suggest novel target genes of *Nrf2* specifically in skeletal muscle. However, because the muscle

samples were harvested from mice 20 weeks after tamoxifen treatment, we cannot rule out the possibility

that these changes in sarcomeric proteins are a consequence of altered redox status following *Nrf2* or

Keap1 KO.
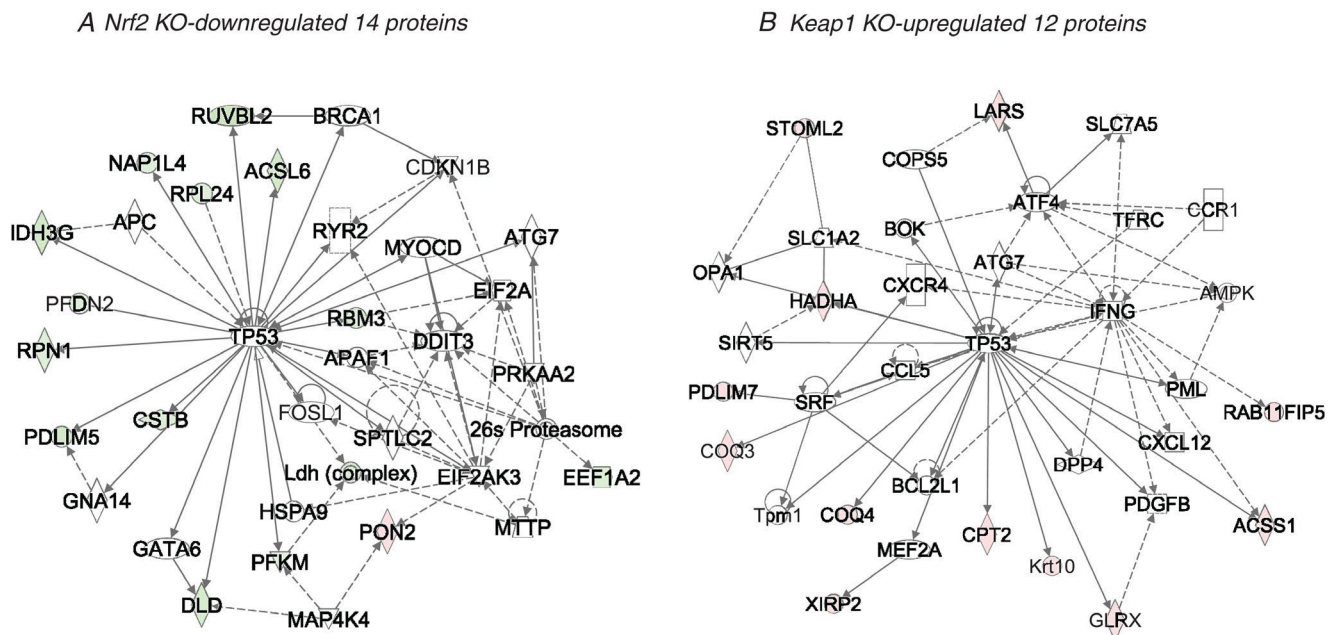
Figure 6. The protein interactive networks between Nrf2 and P53
Nrf2 KO-downregulated proteins (*A*, green) and *Keap1* KO-upregulated proteins (*B*, red) mediate potential inter- action between Nrf2 and P53.

GO analyses suggested that the proteins identified in *Keap1* KO muscle are involved in the

biological processes of NADP metabolism, glutathione metabolism, electron transport chain, drug

metabolism, hydrogen peroxide metabolism and others (Fig. 4*B* and *D*). These processes are critical for

well-known Nrf2 functions, such as antioxidant defence and detoxification. On the other hand, the

proteins identified in *Nrf2* KO muscle are involved in oxidoreduction coenzyme metabolism, purine

ribonucleoside triphosphate metabolism, propanoate metabolism, tryptophan metabolism, myofibril

assembly and regulation of membrane potential. The implications of these changes in Nrf2 functions are not clear at the pre- sent time. Some of these proteins can evoke the metabolic processes that facilitate antioxidant enzyme activity, enhancing the classic Nrf2 function. For example, COQ7 is essential for ubiquinone biosynthesis via converting 6-demethoxyubiquinone to 6-hydroxyubiquinone which is then turned into ubiquinone by the methylase COQ3 (Stenmark *et al*. 2001). COQ7 deficiency results in a total absence of ubiquinone and an accumulation of 6-demethoxyubiquinone (Wang & Hekimi, 2013). HADHA is the alpha subunit of mitochondrial trifunctional protein, which catalyses the last three steps of the mitochondrial beta-oxidation of long-chain fatty acids (Rector *et al*. 2008). An HADHA deficiency results in an accumulation of long-chain fatty acid metabolites (Ibdah *et al*. 2001).

Canonical pathway analysis revealed that four intracellular signalling pathways were activated in Keap1-deficient muscle, including the well-known Nrf2-mediated oxidative stress response, glutathione redox reactions I, glutathione-mediated detoxification and apelin adipocyte signalling pathway (Fig. 5*A*), via upregulating more than 20 pivotal protein components in these pathways (Fig. 5*B*), once again suggesting that the proteins identified in *Keap1* KO muscle mediate the well-recognized Nrf2 functions. However, in Nrf2-deficient muscle we did not find any changes, either activation or inhibition, in the activity of known pathways, suggesting that the function of basal Nrf2 remains to be elucidated. Although this Nrf2-deficient muscle did not demonstrate obvious impairment of antioxidant defence in the basal state, its potential to deal with excessive ROS generated during exercise or other stress conditions should be largely reduced. Accordingly, significantly impaired exercise performance and muscle contractility were observed in the tamoxifen-treated iMS-Nrf2$^{flox/flox}$ mice (Fig. 2).

IPA analysis suggested an overlap of the proteins identified in *Nrf2*- and *Keap1*-KO muscle with the targets of multiple signalling proteins, such as P53, PPARA, Akt, ERK1/2 and TNF (Fig. 6). Particularly for P53, we found that the 14 *Nrf2* KO downregulated proteins and the 12 *Keap1* KO upregulated proteins are involved in the P53 signalling pathway (Fig. 6), suggesting potential synergistic effects and interaction between these two proteins in response to stress challenges. Indeed, P53 has been demonstrated to evoke similar protection as Nrf2 against oxidative stress (Rotblat *et al*. 2012). In skeletal muscle, P53 activates an Nrf2-mediated antioxidant response in order to buffer harmful ROS accumulation (Beyfuss & Hood, 2018). On the other hand, we did not find changes in P53 protein *per se* in Nrf2- or Keap1-deficient muscles either by mass spectrometry or western blotting, suggesting no direct regulation of Nrf2 on P53 protein expression. However, these 26 identified proteins could be potential candidates for studies of crosstalk

between Nrf2 and P53. IPA analysis suggested that the proteins identified in Nrf2- and Keap1-deficient muscles are involved in pathological and physiological processes. *Nrf2* KO-induced downregulation of proteins may result in multiple muscular pathology, such as degeneration of muscle cells (PFKM and HADHA), muscular atrophy (DNM1L), apoptosis of muscle cell lines (PRMT1 and EEF1A2), arrest in cell cycle progression of muscle cell lines (HRAS), and abnormal metabolism (ARNTL, CST3, Pzp, ACADL, HSPA5 and FITM2) (Fig. 7*A*). The IPA analysis also suggested that *Nrf2* KO downregulated six proteins that can result in mitochondrial dysfunction (Fig. 8), such as mitochondrial complex I deficiency (NDUFS6), abnormal morphology of mitochondria (COQ7), volume, length and coupling of mitochondria (AK1), permeability transition of mitochondria (PPID), and transmembrane potential of mitochondria (PHB and YWHAE). Indeed, the *NDUFS6* gene encodes NADH:ubiquinone oxidoreductase subunit S6, which is essential for biogenesis of mitochondrial complex I (Kmita *et al*. 2015). Mutations in this gene cause severe complex I deficiency (Ke *et al*. 2012). *DNM1L* gene encodes dynamin-1-like protein, which is a member of the dynamin superfamily of GTPases and plays a critical role in mitochondrial fission (El-Hattab *et al*. 2018). *PHB* gene encodes prohibitin, a protein in the inner mitochondrial membrane which plays a role in regulating mitochondrial respiration (Artal-Sanz & Tavernarakis, 2009). Our proteomic data show that these mitochondria-associated proteins are significantly down- regulated in Nrf2-deficient skeletal muscle, implying for the first time to our knowledge, that the genes encoding these six proteins are potential targets of Nrf2. Accordingly, it is not surprising that a recent study demonstrated a critical role for Nrf2 in exercise-induced increases in mitochondrial biogenesis of skeletal muscle (Bruns *et al*. 2018).
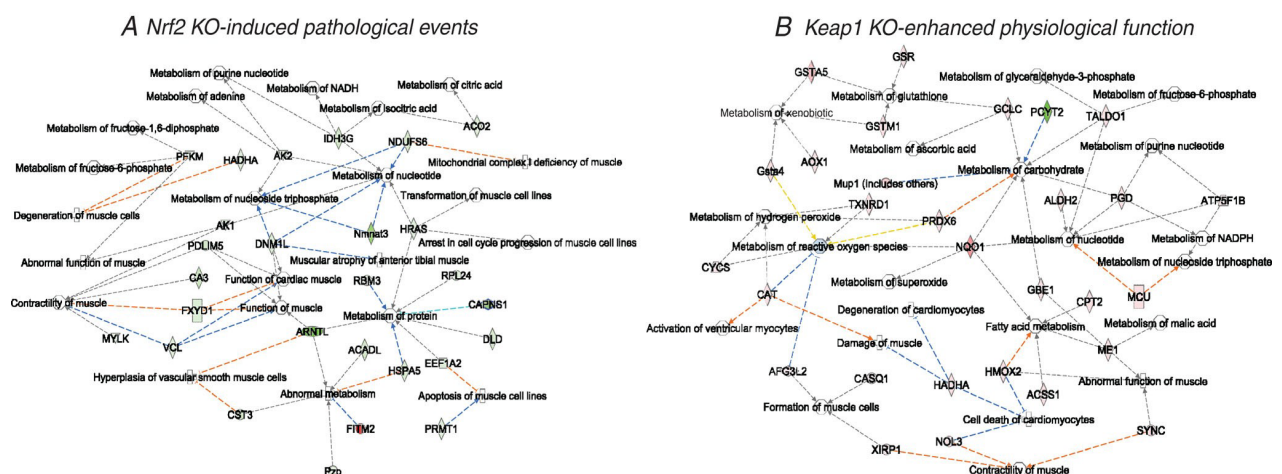

Figure 7. Pathological and physiological networks of proteins identified in *Nrf2*-KO (*A*) and *Keap1*-KO (*B*) skeletal muscle
Nrf2-KO downregulated proteins (*A*, green) leading to multiple dysfunction; *Keap1*-KO-upregulated proteins (*B*, red) improving biological function.

Several proteins identified in *Nrf2*- and *Keap1*-KO muscle participate in the metabolism of glutathione in multiple reactions that are listed in Fig. 9*A*.

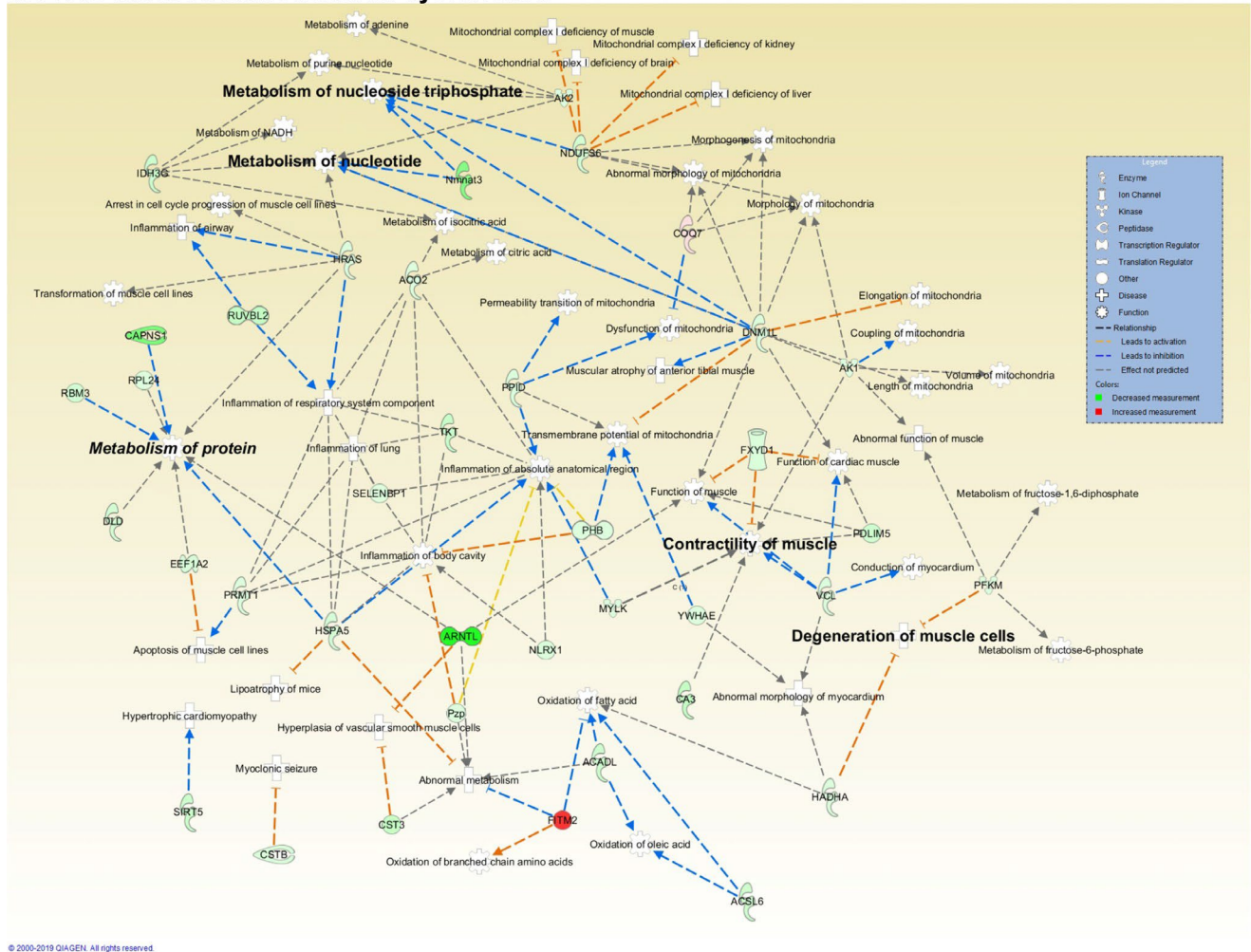**Nrf2 KO-induced mitochondrial dysfunction**

Figure 8. *Nrf2* KO-induced mitochondrial dysfunction [Colour figure can be viewed at wileyonlinelibrary.com]

Employing western blotting, we found a dramatic upregulation of GR, thioredoxin reductase 1 (TrxR1), and glutathione s-transferases A2 (GSTA2) and A4 (GSTA4) in Keap1-deficient Sol muscle, validating data from mass spectrometry. In addition, western blot data further show that these proteins were also upregulated in Keap1-deficient EDL and downregulated in Nrf2-deficient Sol and EDL (Fig. 9*B*). These alterations were not detected by mass spectrometry, suggesting some false-negative results in the proteomic analysis. Although the influence of GR/TrxR1 and Grx/GSTs on glutathione metabolism were opposite, our data show that the regulation of the Nrf2/Keap1 system on these enzymes are in the same direction. For example, *Keap1* deletion markedly upregulated not only GR/TrxR1, but also Grx/GSTs, implying both oxidation and reduction potential of glutathione are enhanced when *Nrf2* is activated. This is an intriguing phenomenon but its functional significance is not clear. However, GSH but not GSSG, were

significantly increased and decreased in the *Keap1*- and *Nrf2*-KO muscles, respectively, suggesting that the net effects of *Nrf2* activation on glutathione status is to enhance antioxidant capacity of the glutaredoxin system. Interestingly, a similar change in glutathione status has been found in plasma, suggesting an influence of skeletal muscle Nrf2/Keap1 on systemic oxidative status and supporting the concept that skeletal muscle functions as an endocrine organ (Pedersen, 2013; Giudice & Taylor, 2017; Hoffmann & Weigert, 2017). Although it has been suggested that skeletal muscle can influence the central nervous system during exercise by inter-organ crosstalk (Delezie & Handschin, 2018; Pedersen, 2019), we did not find significant changes in the brainstem glutathione status of these mice.
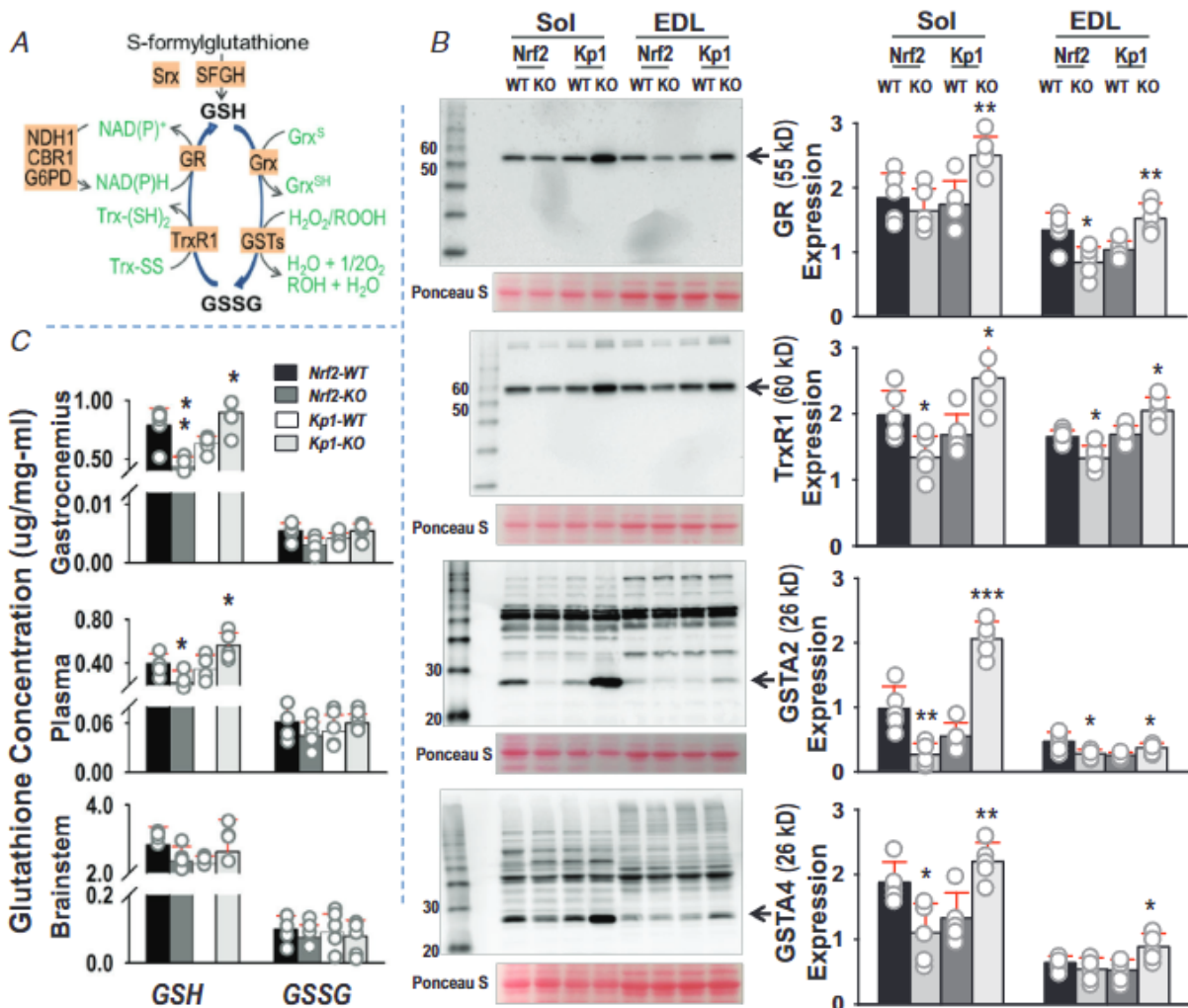
Figure 9. Change in skeletal muscle glutaredoxin system following *Nrf2* or *Keap1* deletion
A, glutaredoxin system-associated proteins identified in *Nrf2* KO or *Keap1* KO muscle. *B*, western blot analysis confirmed the altered expression of GR, TrxR1, GSTA2 and GSTA4. Data are shown as the mean ± SD, with individual data points ($n = 5$). *$P < 0.05$, **$P < 0.01$, knockout (KO) *vs.* wild-type (WT) with unpaired *t* test by SigmaPlot software. *C*, glutathione (Glu) in gastrocnemius, plasma and brainstem. Data are shown as the mean ± SD, with individual data points ($n = 5$). *$P < 0.05$, **$P < 0.01$, KO *vs*. WT with unpaired *t* test by SigmaPlot software. [Colour figure can be viewed at wileyonlinelibrary.com]

Proteomic and bioinformatic analyses also suggested that several proteins essential for normal mitochondrial function were downregulated when *Nrf2* was deleted (Fig. 4*C*). Accordingly, we further evaluated mitochondrial quantity and quality in skeletal muscle following Nrf2- or Keap1-deficiency. We found that Nrf2-deficient muscle displayed low CS activity (Fig. 10*A*) and downregulated respiratory chain complex protein expression (Fig. 10*B*), suggesting reduced mitochondrial content. Moreover, we further found that Sol mitochondrial respiratory function, specifically complex I and complex I+II state 3 were significantly reduced in *Nrf2*-KO compared with *Nrf2*-WT, *Keap1*-KO and *Keap1*-WT. However, there were no differences in mitochondrial respiratory function in *Nrf2*-WT *vs.* *Keap1*-KO *vs.* *Keap1*-WT (Fig. 10*C*). These findings indicate that Nrf2 deficiency may attenuate mitochondrial respiratory function by reducing complex I-mediated oxidative phosphorylation, and reduced complex I+II state 3 respiration is also primarily due to attenuated complex I state 3 respiration without any difference in complex II respiration. We also found that Keap1 deletion does not affect mitochondrial respiratory function. Reduced mitochondrial respiratory function may be explained by reduced protein expression of complex I in *Nrf2*-KO compared with *Nrf2*-WT, *Keap1*-KO and *Keap1*-WT. Furthermore, our proteomic data (Fig. 5*C*) showed that Nrf2 deficiency attenuated mitochondrial complex I respiratory function-associated proteins. These data provide evidence that Nrf2 deficiency leads to mitochondrial dysfunction in skeletal muscle. We and others have previously reported that Nrf2 deficiency in mice results in elevated ROS and reduced SOD2 protein expression (Miller *et al*. 2012; Kitaoka *et al*. 2016) that may be mediated by an increase in mitochondrial DNA damage (Wang *et al*. 2016; Coleman *et al*. 2018) and decrease in protein expression of mitochondrial respiratory complexes that lead to mitochondrial respiratory dysfunction (Fig. 10). Importantly, previous studies suggest that increased oxidative stress by Nrf2 deficiency increases mitochondrial fragmentation and toxicity, which lead to mitochondrial dysfunction (Gao *et al*. 2001; Higgins & Hayes, 2011; Zhang *et al*. 2011). Kitaoka *et al*. (2019) recently reported that Nrf2 deficiency downregulated mitochondrial fusion regulation genes, which was also found in our proteomic data (Fig. 5*C*). Nrf2 deficiency downregulated proteins encoded by the genes NDUFS6, DNM1L, Ak1, PPID, PHB and YWHAE are associated with mitochondrial respiratory function (Kitaoka et al. 2019). These findings further support the concept that elevated oxidative damage mediated by Nrf2 deficiency leads to mitochondrial dysfunction.
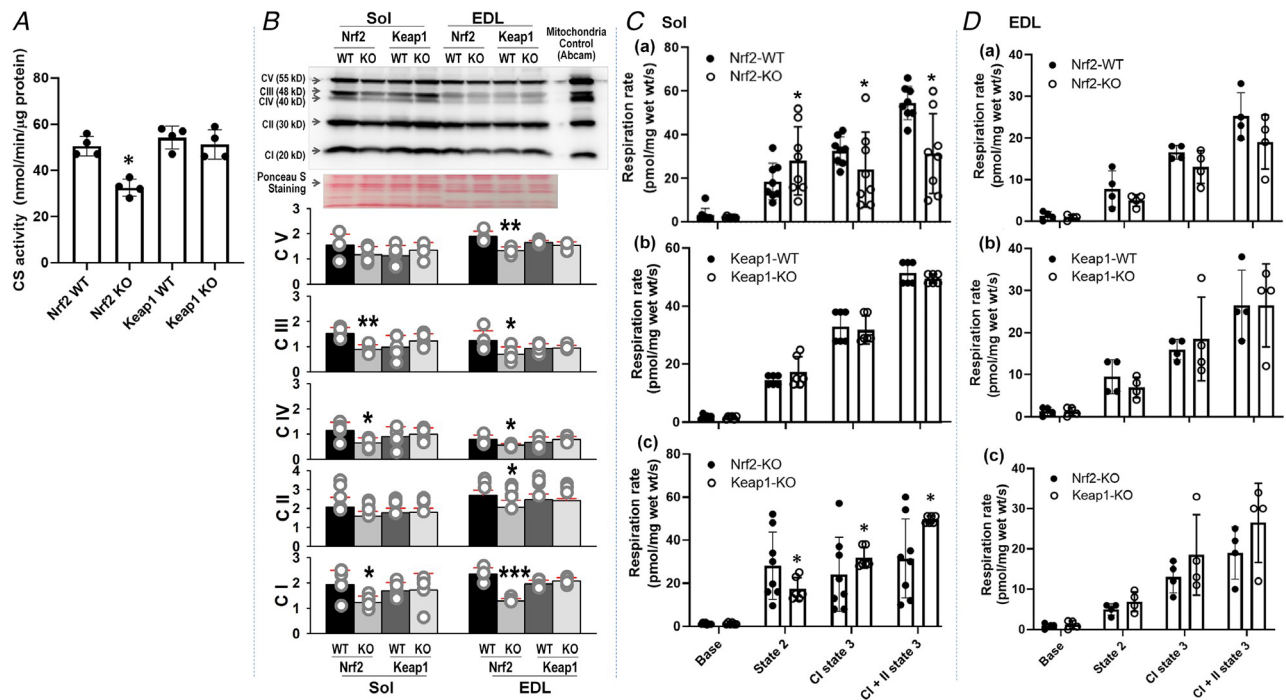
Figure 10. Mitochondrial content and function
A, citrate synthase activity of the soleus (Sol). Data are shown as the mean ± SD, with individual data points (n = 4). ∗P < 0.05, knockout (KO) vs. wild-type (WT) with unpaired t test by SigmaPlot software. B, western blot analysis of mitochondrial respiratory complex protein levels. Data are shown as the mean ± SD, with individual data points (n = 5). ∗P < 0.05, ∗∗P < 0.01, ∗∗∗P < 0.001, KO vs. WT with unpaired t test by SigmaPlot software. C, mitochondrial respiratory complex function of Sol. Data are shown as the mean ± SD, with individual data points (n = 8). ∗P < 0.05, KO vs. WT with unpaired t test by SigmaPlot software. D, mitochondrial respiratory complex function of extensor digitorum longus (EDL). Data are shown as the mean ± SD, with individual data points (n = 4). No statistically significant difference between KO and WT groups was found. [Colour figure can be viewed at wileyonlinelibrary.com]

We also assessed mitochondrial respiratory function in EDL; however, Nrf2 deletion in this muscle did not show statistical differences ($P = 0.08$) in mitochondrial respiratory function compared with other conditions. This may be due to the fact that the EDL contains fewer mitochondria than the Sol. Although we have utilized a high-resolution respirometer, there are technical limitations when measuring respiration from smaller tissues that contain few mitochondria such as the EDL. However, we did observe a trend that mitochondrial complex I state 3 was somewhat lower in *Nrf2*-KO mice. This warrants further investigation using larger tissues or isolated mitochondrial methods. Finally, Nrf2 deficiency in EDL may rely on different signalling pathways or respond differently compared with the Sol, since muscle fibre types are markedly different (Kitaoka *et al*. 2019).

In summary, employing two transgenic mouse models selectively aimed at skeletal muscle Nrf2/Keap1, we demonstrated that Nrf2 is essential for normal muscle function and when it was upregulated by deleting *Keap1*, exercise performance and skeletal muscle contractility were markedly improved. Proteomic and bioinformatic analyses of the Keap1-deficient skeletal muscles confirmed the well-recognized antioxidant defence induced by Nrf2. On the other hand, the data from Nrf2-deficient muscle revealed some novel target proteins, signalling pathways, and molecular networks of Nrf2 that need to be further elucidated. One major limitation of this study is the small sample size available for mass spectrometric analysis ($n = 3$/group) that may lead to a false negative result for some proteins. Other limitations relate to the time points of model induction and tissue sampling. Gene deletion of *Nrf2* or *Keap1* in the present experiment was induced at 3 months of age that may affect muscle/animal development, although no gross phenotypic changes were observed. Twenty weeks of gene deficiency may evoke compensatory mechanisms that mask some effects of gene knockout *per se*. Nevertheless, these data are the first to our knowledge to describe functional alterations and protein profiles after manipulating the Nrf2/Keap1 system selectively in skeletal muscle.
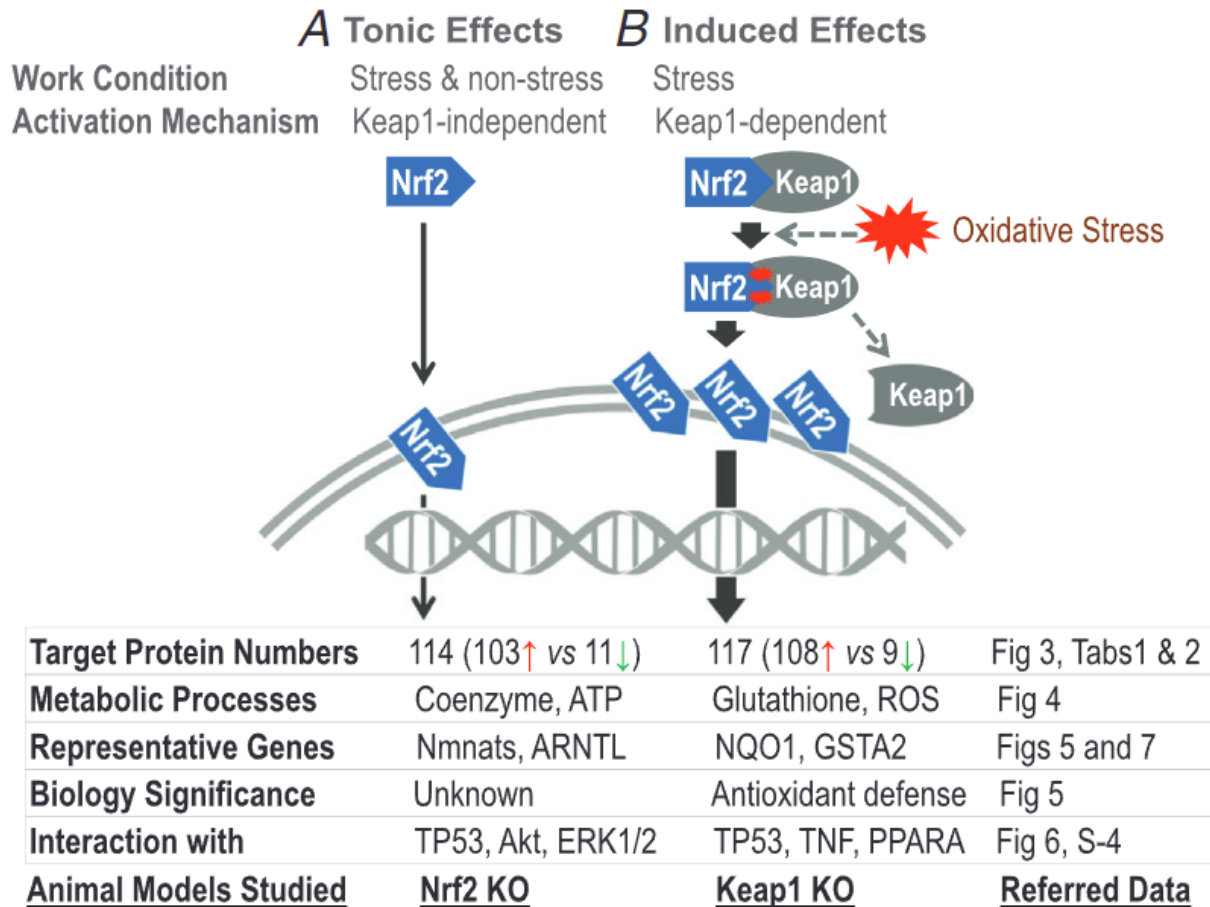
Figure 11. Two-way model of Nrf2 function
A, tonic effects induced by low level Nrf2 that are independent on Keap1. *B*, induced effects in response to stress challenges that are evoked by a surge of Nrf2 *via* Keap1-dependent mechanism. ↑ gene upregulation; ↓ gene downregulation. [Colour figure can be viewed at wileyonlinelibrary.com]

Recently, two studies reported skeletal muscle-specific *Nrf2* or *Keap1* KO mouse models. Uruno *et al*. (2016) utilized a microarray to assay gene expression of skeletal muscle deficient of Keap1. Yamada *et al*. (2019) determined well-known Nrf2 target proteins in skeletal muscle after *Nrf2* was deleted. Compared with these papers, our data provide a broader view of Nrf2 functional significance by revealing several new target proteins, signalling pathways and molecular networks. We uniquely accessed the functional significance of skeletal muscle KO of both Nrf2 and Keap1 under similar experimental conditions.

It is apparent that the proteins we found that were downregulated in *Nrf2*-KO muscle represent one category of Nrf2 targets whose expression strictly relies on basal Nrf2 activity. On the other hand, the proteins upregulated in *Keap1*-KO muscle represent another group of targets whose expression is provoked by high levels of Nrf2. When *Keap1* is deleted, all of Nrf2 targeted proteins are liberated from the inhibition that represents the maximal response of Nrf2 in the face of oxidative stress challenges that occurred under

the conditions of our study. Accordingly, we propose a two-way model of Nrf2 function, which is shown in Fig. 11: (1) a tonic effect maintained by a constant low level of Nrf2 for basal biological processes such as ATP generation and mitochondrial respiration that are independent on Keap1 regulation; and (2) an inducible effect mediated by a surge of Nrf2 liberated from Keap1 to evoke antioxidant defences or other cyto-protective responses to oxidative stress.

References

Ahn B, Pharaoh G, Premkumar P, Huseman K, Ranjit R, Kinter M, Szweda L, Kiss T, Fulop G, Tarantini S, Csiszar A, Ungvari Z & Van Remmen H (2018). Nrf2 deficiency exacerbates age-related contractile dysfunction and loss of skeletal muscle mass. *Redox Biol* **17**, 47–58.

Artal-Sanz M & Tavernarakis N (2009). Prohibitin and mitochondrial biology. *Trends Endocrinol Metab* **20**, 394–401.

Benjamini Y & Hochberg Y (1995). Controlling the false discovery rate: a practical and powerful approach to multiple testing. *JR Stat Soc Series B Methodol* **57**, 289–300.

Beyfuss K & Hood DA (2018). A systematic review of p53 regulation of oxidative stress in skeletal muscle. *Redox Rep* **23**, 100–117.

Bindea G, Mlecnik B, Hackl H, Charoentong P, Tosolini M, Kirilovsky A, Fridman WH, Pages F, Trajanoski Z & Galon J (2009). ClueGO: a Cytoscape plug-in to decipher functionally grouped gene ontology and pathway annotation networks. *Bioinformatics* **25**, 1091–1093.

Brooks HL & Lindsey ML (2018). Guidelines for authors and reviewers on antibody use in physiology studies. *Am J Physiol Heart Circ Physiol* **314**, H724-H732.

Bruns DR, Drake JC, Biela LM, Peelor FF, 3rd, Miller BF & Hamilton KL (2015). Nrf2 signaling and the slowed aging phenotype: evidence from long-lived models. *Oxid Med Cell Longev* **2015**, 1.

Bruns DR, Ehrlicher SE, Khademi S, Biela LM, Peelor FF, 3rd, Miller BF & Hamilton KL (2018). Differential effects of vitamin C or protandim on skeletal muscle adaptation to exercise. *J Appl Physiol* **125**, 661–671.

Coleman V, Sa-Nguanmoo P, Koenig J, Schulz TJ, Grune T, Klaus S, Kipp AP & Ost M (2018). Partial involvement of Nrf2 in skeletal muscle mitohormesis as an adaptive response to mitochondrial uncoupling. *Sci Rep* **8**, 2446.

Crilly MJ, Tryon LD, Erlich AT & Hood DA (2016). The role of Nrf2 in skeletal muscle contractile and mitochondrial function. *J Appl Physiol* **121**, 730–740.

Cuadrado A, Manda G, Hassan A, Alcaraz MJ, Barbas C, Daiber A, Ghezzi P, Leon R, Lopez MG, Oliva B, Pajares M, Rojo AI, Robledinos-Anton N, Valverde AM, Guney E & Schmidt H (2018). Transcription factor NRF2 as a therapeutic target for chronic diseases: A systems medicine approach. *Pharmacol Rev* **70**, 348–383.

Cuadrado A, Rojo AI, Wells G, Hayes JD, Cousin SP, Rumsey WL, Attucks OC, Franklin S, Levonen AL, Kensler TW & Dinkova-Kostova AT (2019). Therapeutic targeting of the NRF2 and KEAP1 partnership in chronic diseases. *Nat Rev Drug Discov* **18**, 295-317,

Davies KJ, Quintanilha AT, Brooks GA & Packer L (1982). Free radicals and tissue damage produced by exercise. *Biochem Biophys Res Commun* **107**, 1198–1205.

Delezie J & Handschin C (2018). Endocrine crosstalk between skeletal muscle and the brain. *Front Neurol* **9**, 698.

Duthie GG, Robertson JD, Maughan RJ & Morrice PC (1990). Blood antioxidant status and

erythrocyte lipid peroxidation following distance running. *Arch Biochem Biophys* **282**, 78–83.

El-Hattab AW, Suleiman J, Almannai M & Scaglia F (2018). Mitochondrial dynamics: biological roles, molecular machinery, and related diseases. *Mol Genet Metab* **125**, 315–321.

Gao X, Dinkova-Kostova AT & Talalay P (2001). Powerful and prolonged protection of human retinal pigment epithelial cells, keratinocytes, and mouse leukemia cells against oxidative damage: the indirect antioxidant effects of sulforaphane. *Proc Natl Acad Sci U S A* **98**, 15221–15226.

Gifford JR, Trinity JD, Layec G, Garten RS, Park SY, Rossman MJ, Larsen S, Dela F & Richardson RS (2015). Quadriceps exercise intolerance in patients with chronic obstructive pulmonary disease: the potential role of altered skeletal muscle mitochondrial respiration. *J Appl Physiol* **119**, 882–888.

Giudice J & Taylor JM (2017). Muscle as a paracrine and endocrine organ. *Curr Opin Pharmacol* **34**, 49–55.

Gnaiger E (2009). Capacity of oxidative phosphorylation in human skeletal muscle: new perspectives of mitochondrial physiology. *Int J Biochem Cell Biol* **41**, 1837–1845.

Granzier H, Helmes M, Cazorla O, McNabb M, Labeit D, Wu Y, Yamasaki R, Redkar A, Kellermayer M, Labeit S & Trombitas K (2000). Mechanical properties of titin isoforms. *Adv Exp Med Biol* **481**, 283–300; discussion 300-284.

Hayes JD & Dinkova-Kostova AT (2014). The Nrf2 regulatory network provides an interface between redox and intermediary metabolism. *Trends Biochem Sci* **39**, 199–218.

Higgins LG & Hayes JD (2011). The cap'n'collar transcription factor Nrf2 mediates both intrinsic resistance to environmental stressors and an adaptive response elicited by chemopreventive agents that determines susceptibility to electrophilic xenobiotics. *Chem Biol Interact* **192**, 37–45.

Hodge BA, Wen Y, Riley LA, Zhang X, England JH, Harfmann BD, Schroder EA & Esser KA (2015). The endogenous molecular clock orchestrates the temporal separation of substrate metabolism in skeletal muscle. *Skelet Muscle* **5**, 17.

Hoffmann C & Weigert C (2017). Skeletal muscle as an endocrine organ: the role of myokines in exercise adaptations. *Cold Spring Harb Perspect Med* **7**, a029793.

Horie M, Warabi E, Komine S, Oh S & Shoda J (2015). Cytoprotective role of Nrf2 in electrical pulse stimulated C2C12 myotube. *PLoS One* **10**, e0144835.

Ibdah JA, Paul H, Zhao Y, Binford S, Salleng K, Cline M, Matern D, Bennett MJ, Rinaldo P & Strauss AW (2001). Lack of mitochondrial trifunctional protein in mice causes neonatal hypoglycemia and sudden death. *J Clin Invest* **107**, 1403–1409.

Jackson MJ (2008). Free radicals generated by contracting muscle: by-products of metabolism or key regulators of muscle function? *Free Radic Biol Med* **44**, 132–141.

Jackson MJ (2011). Control of reactive oxygen species production in contracting skeletal muscle. *Antioxid Redox Signal* **15**, 2477–2486.

Kanter M (1998). Free radicals, exercise and antioxidant supplementation. *Proc Nutr Soc* **57**, 9–13.

Ke BX, Pepe S, Grubb DR, Komen JC, Laskowski A, Rodda FA, Hardman BM, Pitt JJ, Ryan MT, Lazarou M, Koleff J, Cheung MM, Smolich JJ & Thorburn DR (2012). Tissue-specific splicing of an Ndufs6 gene-trap insertion generates a mitochondrial complex I deficiency-specific cardiomyopathy. *Proc Natl Acad Sci U S A* **109**, 6165–6170.

Kitaoka Y, Takeda K, Tamura Y, Fujimaki S, Takemasa T & Hatta H (2016). Nrf2 deficiency does not affect denervation-induced alterations in mitochondrial fission and fusion proteins in skeletal muscle. *Physiol Rep* **4**, e13064.

Kitaoka Y, Tamura Y, Takahashi K, Takeda K, Takemasa T & Hatta H (2019). Effects of Nrf2 deficiency on mitochondrial oxidative stress in aged skeletal muscle. *Physiol Rep* **7**, e13998.

Kmita K, Wirth C, Warnau J, Guerrero-Castillo S, Hunte C, Hummer G, Kaila VR, Zwicker K, Brandt U & Zickermann V (2015). Accessory NUMM (NDUFS6) subunit harbors a Zn-binding site and is essential for biogenesis of mitochondrial complex I. *Proc Natl Acad Sci U S A* **112**, 5685–5690.

Kong X, Thimmulappa R, Craciun F, Harvey C, Singh A, Kombairaju P, Reddy SP, Remick D & Biswal S (2011). Enhancing Nrf2 pathway by disruption of Keap1 in myeloid leukocytes protects against sepsis. *Am J Respir Crit Care Med* **184**, 928–938.

Lee JM, Li J, Johnson DA, Stein TD, Kraft AD, Calkins MJ, Jakel RJ & Johnson JA (2005). Nrf2, a multi-organ protector? *FASEB J* **19**, 1061–1066.

Li T, He S, Liu S, Kong Z, Wang J & Zhang Y (2015). Effects of different exercise durations on Keap1-Nrf2-ARE pathway activation in mouse skeletal muscle. *Free Radic Res* **49**, 1269–1274.

McArdle A, Pattwell D, Vasilaki A, Griffiths RD & Jackson MJ (2001). Contractile activity-induced oxidative stress: cellular origin and adaptive responses. *Am J Physiol Cell Physiol* **280**, C621-C627.

McCarthy JJ, Srikuea R, Kirby TJ, Peterson CA & Esser KA (2012). Inducible Cre transgenic mouse strain for skeletal muscle-specific gene targeting. *Skelet Muscle* **2**, 8.

McDonagh B (2016). Redox regulation in skeletal muscle aging and exercise. *Front Physiol* **7**, 5.

Merry TL & Ristow M (2016). Nuclear factor erythroid-derived 2-like 2 (NFE2L2, Nrf2) mediates exercise-induced mitochondrial biogenesis and the anti-oxidant response in mice. *J Physiol* **594**, 5195–5207.

Miller CJ, Gounder SS, Kannan S, Goutam K, Muthusamy VR, Firpo MA, Symons JD, Paine R, 3rd, Hoidal JR & Rajasekaran NS (2012). Disruption of Nrf2/ARE signaling impairs antioxidant mechanisms and promotes cell degradation pathways in aged skeletal muscle. *Biochim Biophys Acta* **1822**, 1038–1050.

Mondal A & Jin J-PJFiP (2016). Protein structure-function relationship at work: learning from myopathy mutations of the slow skeletal muscle isoform of troponin T. *Front Physiol* **7**, 449.

Mukund K & Subramaniam S (2019). Skeletal muscle: A review of molecular structure and function, in health and disease. *Wiley Interdiscip Rev Syst Biol Med* **12**, e1462.

Osburn WO & Kensler TW (2008). Nrf2 signaling: an adaptive response pathway for protection against environmental toxic insults. *Mutat Res* **659**, 31–39.

Park SY, Gifford JR, Andtbacka RH, Trinity JD, Hyngstrom JR, Garten RS, Diakos NA, Ives SJ, Dela

F, Larsen S, Drakos S & Richardson RS (2014). Cardiac, skeletal, and smooth muscle mitochondrial respiration: are all mitochondria created equal? *Am J Physiol Heart Circ Physiol* **307**, H346-H352.

Park SY, Rossman MJ, Gifford JR, Bharath LP, Bauersachs J, Richardson RS, Abel ED, Symons JD & Riehle C (2016). Exercise training improves vascular mitochondrial function. *Am J Physiol Heart Circ Physiol* **310**, H821-H829.

Pattwell DM, McArdle A, Morgan JE, Patridge TA & Jackson MJ (2004). Release of reactive oxygen and nitrogen species from contracting skeletal muscle cells. *Free Radic Biol Med* **37**, 1064–1072.

Pedersen BK (2013). Muscle as a secretory organ. *Compr Physiol* **3**, 1337–1362.

Pedersen BK (2019). Physical activity and muscle–brain crosstalk. *Nat Rev Endocrinol* **15**, 383-392,

Powers SK & Hamilton K (1999). Antioxidants and exercise. *Clin Sports Med* **18**, 525–536.

Powers SK & Jackson MJ (2008). Exercise-induced oxidative stress: cellular mechanisms and impact on muscle force production. *Physiol Rev* **88**, 1243–1276.

Powers SK, Radak Z & Ji LL (2016). Exercise-induced oxidative stress: past, present and future. *J Physiol* **594**, 5081–5092.

Rector RS, Payne RM & Ibdah JA (2008). Mitochondrial trifunctional protein defects: clinical implications and therapeutic approaches. *Adv Drug Deliv Rev* **60**, 1488–1496.

Reid MB, Haack KE, Franchek KM, Valberg PA, Kobzik L & West MS (1992*a*). Reactive oxygen in skeletal muscle. I. Intracellular oxidant kinetics and fatigue in vitro. *J Appl Physiol* **73**, 1797–1804.

Reid MB, Shoji T, Moody MR & Entman ML (1992*b*). Reactive oxygen in skeletal muscle. II. Extracellular release of free radicals. *J Appl Physiol* **73**, 1805–1809.

Rotblat B, Melino G & Knight RA (2012). NRF2 and p53: Januses in cancer? *Oncotarget* **3**, 1272–1283.

Shannon P, Markiel A, Ozier O, Baliga NS, Wang JT, Ramage D, Amin N, Schwikowski B & Ideker T (2003). Cytoscape: a software environment for integrated models of biomolecular interaction networks. *Genome Res* **13**, 2498–2504.

Steinbacher P & Eckl P (2015). Impact of oxidative stress on exercising skeletal muscle. *Biomolecules* **5**, 356–377.

Stenmark P, Grunler J, Mattsson J, Sindelar PJ, Nordlund P & Berthold DA (2001). A new member of the family of di-iron carboxylate proteins. Coq7 (clk-1), a membrane-bound hydroxylase involved in ubiquinone biosynthesis. *J Biol Chem* **276**, 33297–33300.

Urso ML & Clarkson PM (2003). Oxidative stress, exercise, and antioxidant supplementation. *Toxicology* **189**, 41–54.

Uruno A, Yagishita Y, Katsuoka F, Kitajima Y, Nunomiya A, Nagatomi R, Pi J, Biswal SS & Yamamoto M (2016). Nrf2-Mediated Regulation of Skeletal Muscle Glycogen Metabolism. *Mol Cell Biol* **36**, 1655–1672.

Wafi AM, Hong J, Rudebush TL, Yu L, Hackfort BT, Wang HJ, Schultz HD, Zucker IH & Gao L (2018). Curcumin improves exercise performance of mice with coronary artery ligation induced HFrEF: Nrf2 and antioxidant mechanisms in skeletal muscle. *J Appl Physiol* **126**, 477–486.

Wang P, Li CG, Qi Z, Cui D & Ding S (2016). Acute exercise stress promotes Ref /Nrf signaling and increases mitochondrial antioxidant activity in skeletal muscle. *Exp Physiol* **101**, 410–420

Wang Y & Hekimi S (2013). Mitochondrial respiration without ubiquinone biosynthesis. *Hum Mol Genet* **22**, 4768–4783.

Yamada M, Iwata M, Warabi E, Oishi H, Lira VA & Okutsu M (2019). p62/SQSTM1 and Nrf2 are essential for exercise-mediated enhancement of antioxidant protein expression in oxidative muscle. *FASEB J* **33**, 8022–8032.

Yamamoto M, Kensler TW & Motohashi H (2018). The KEAP1-NRF2 system: a thiol-based sensor-effector apparatus for maintaining redox homeostasis. *Physiol Rev* **98**, 1169–1203.

Zhang Y, Ahn YH, Benjamin IJ, Honda T, Hicks RJ, Calabrese V, Cole PA & Dinkova-Kostova AT (2011). HSF1-dependent upregulation of Hsp70 by sulfhydryl-reactive inducers of the KEAP1/NRF2/ARE pathway. *Chem Biol* **18**, 1355–1361.

Additional information

Data availability statement

All data that support the findings of this study are openly available in figshare at https://doi.org/10.6084/m9.figshare. 12808421.v1

Competing interests

None declared.

Author contributions

L.G. and I.H.Z. conceived the project with input from H.J.W. and H.D.S.; V.K. performed proteomic analysis;

N.N.V. performed bioinformatics analysis with consults from P.X. and C.G.; L.G., I.H.Z., T.L.R. and L.Y. created the mouse models with the management of animal breading by T.L.R. and carried on genotyping assay and western blot analyses by L.Y; S.Y.P., W.M.S. and E.J.P. evaluated mitochondrial content and mitochondrial respiratory complex function. L.G., A.M.W. and J.H. performed exercise capacity and skeletal muscle contractility evaluation. L.G. and I.H.Z. co-wrote the article. All authors edited the article.

Keywords

bioinformatics, Nrf2/Keap1, proteomics, skeletal muscle, tissue-specific transgenic mice

Supporting information

Additional supporting information may be found online in the Supporting Information section at the end of the article.

Statistical Summary Document